Palaeogeography, Palaeoclimatology, Palaeoecology 463 (2016) 45–59

Contents lists available at ScienceDirect

Palaeogeography, Palaeoclimatology, Palaeoecology

journal homepage: www.elsevier.com/locate/palaeo

Microfossil turnover across the uppermost Danian at Caravaca, Spain: Paleoenvironmental inferences and identification of the latest Danian event

Laia Alegret [a,b,*], Silvia Ortiz [c], Gabriela J. Arreguín-Rodríguez [a], Simonetta Monechi [d], Isabel Millán [e], Eustoquio Molina [a,b]

[a] Departamento de Ciencias de la Tierra, Universidad de Zaragoza, Pedro Cerbuna 12, 50009, Zaragoza, Spain
[b] Instituto Universitario de Ciencias Ambientales, Universidad de Zaragoza, Zaragoza, Spain
[c] PetroStrat Ltd., Tan-y-Graig, Parc Caer Seion, Conwy, Wales LL32 8FA, UK
[d] Dipartimento di Scienze della Terra, Università di Firenze, Via La Pira 4, 50121 Firenze, Italy
[e] TNO Petroleum Geoscience, Princetonlaan 6, 3584 CB Utrecht, The Netherlands

ARTICLE INFO

Article history:
Received 9 May 2016
Received in revised form 16 September 2016
Accepted 19 September 2016
Available online 22 September 2016

Keywords:
Upper Danian
Hyperthermal
Microfossils
Carbonate corrosivity
Food-flux

ABSTRACT

The Latest Danian Event (LDE) or Top Chron C27n hyperthermal event has been identified in the Caravaca section (Southern Spain) by means of calcareous nannofossil biozones (Subzone NTp7b) and the recognition of a prominent, negative ~0.6 per mille carbon isotope excursion measured in benthic foraminiferal tests. This is the first time that this Danian hyperthermal event has been identified in a deep-water, middle to lower bathyal setting from the Western Tethyan realm.

The analysis of benthic foraminiferal assemblages shows gradual changes in the assemblages prior to the onset of the LDE and an increase in food supply to the seafloor during the LDE, in agreement with results from shallower Southern Tethyan settings. The benthic assemblage changes across the LDE at Caravaca share some characteristics with other hyperthermal events, including the negative carbon isotope excursion, the increased abundance of buliminids, or the common occurrence of *A. aragonensis*, an opportunistic species that proliferated during other Paleogene hyperthermal events. In addition, the increased abundance of *Nuttallides truempyi*, a dissolution-resistant form that thrived during the Paleocene Eocene Thermal Maximum, and the abundance of calcareous infaunal morphogroups, which calcify in less carbonate-undersaturated pore waters, indicate slightly $CaCO_3$-corrosive bottom waters during the LDE.

Turnover of calcareous plankton across the LDE is similar to other sites globally distributed, including the evolution of photosymbiotic foraminiferal lineages and the radiation of the nannofossil "fasciculiths group". The occurrence of innovative morphostructures (*Diantholitha* and *Lithoptychius*) towards the base of the LDE may indicate a more efficient biological pump. This hypothesis is supported by increased percentages of benthic infaunal morphogroups and a decrease in the abundance of oligotrophic species.

A reworked interval has been identified immediately above the LDE. Higher up in the section, benthic and planktic assemblages from the post-LDE interval point to the recovery of the environmental conditions, including a decrease in the food supply to the seafloor.

1. Introduction

The early Paleogene was a dynamic part of the geological record, characterised by a long-term global warming trend (Zachos et al., 2001) punctuated by short-lived perturbations of the carbon cycle that have been linked to extreme (1–4 °C) warming pulses, called hyperthermals (e.g. Littler et al., 2014). The Paleocene-Eocene Thermal Maximum (PETM, ~56 Ma) was the largest hyperthermal event: temperatures increased globally by 5 to 9 °C within <10,000 years (e.g. Röhl et al., 2000; Zachos et al., 2006; Thomas, 2007) and mean deep-sea temperatures increased by 5 °C (Dunkley-Jones et al., 2013). The biotic consequences of the PETM include diversification and migrations in the oceans and on land, while deep-sea benthic foraminifera suffered from the largest extinction (30–55% of the species) in the Phanerozoic (e.g. Tjalsma and Lohmann, 1983; Thomas, 2007; Alegret et al., 2009a, 2009b, 2010). The PETM and the abrupt ~3–4‰ carbon isotope excursion (CIE) at the base of the event have been associated with a massive release of methane with strongly depleted carbon isotope signature

* Corresponding author at: Dept. Ciencias de la Tierra, Universidad de Zaragoza. Calle Pedro Cerbuna, 12, 50009 Zaragoza, Spain.
E-mail address: laia@unizar.es (L. Alegret).

http://dx.doi.org/10.1016/j.palaeo.2016.09.013
0031-0182/

($\delta^{13}C$) (Dickens et al., 1995; Bowen et al., 2014), but the triggering mechanism of the methane release is still under debate and includes such causes as the crossing of a climatic threshold (e.g. Lourens et al., 2005), organic matter oxidation (Higgins and Schrag, 2006), burning of peat deposits (Kurtz et al., 2003), increased volcanic activity in the North Atlantic Igneous Province (Svensen et al., 2004; Nisbet et al., 2009), and orbitally forced dissociation of permafrost deposits on Antarctica (DeConto et al., 2012).

The PETM shares characteristics with other early Eocene hyperthermals (e.g. ETM 1 to 3), including CIEs in carbonate and organic matter, oxygen isotope ($\delta^{18}O$) excursions indicative of warming, dissolution of deep-sea marine carbonates, increased continental weathering and biotic perturbations (e.g. Thomas and Zachos, 2000; Nicolo et al., 2007; Stap et al., 2010; Lauretano et al., 2015; Arreguín-Rodríguez et al., 2016; Arreguín-Rodríguez and Alegret, 2016). Hyperthermal events of smaller magnitude have also been reported from the Paleocene, and these include the Dan-C2 event (Quillévéré et al., 2008; also called Lower C29n event, Coccioni et al., 2010), the Top C27n event (also called Latest Danian Event, LDE; Bornemann et al., 2009; Westerhold et al., 2008), or possibly the Early Late Paleocene Event (ELPE, Petrizzo, 2005; also called Mid Paleocene Biotic Event, MPBE, Bernaola et al., 2007).

Whereas the PETM has been intensively studied over the last decades, the exact timing, magnitude and pattern of other hyperthermals as well as their paleoenvironmental consequences are still poorly understood, and further studies are necessary for correlation purposes and to look into the origin of the transient greenhouse episodes, especially during the Paleocene. Here we focus on the Top C27n event (Westerhold et al., 2008) or Latest Danian Event (LDE; Bornemann et al., 2009) at ~62.15 Ma (Dinarès-Turell et al., 2014). This ~2–3 °C transient warming event is associated with a 0.5–2‰ CIE and it has been identified in the central Pacific Ocean (Shatsky Rise, Westerhold et al., 2011), NE Atlantic Ocean (Zumaia section in Spain, Dinarès-Turell et al., 2012), Caribbean Sea and SE Atlantic Ocean (Westerhold et al., 2008), Southern Tethyan shelf (Egypt and Tunisia, Bornemann et al., 2009; Sprong et al., 2013) and Northern Tethys (Bjala section in Bulgaria, Dinarès-Turell et al., 2012). Reported similarities between the LDE and the PETM include a relatively rapid onset of the CIE and a longer tailing back to pre-event values, and an estimated duration of ~200 ka (Dinarès-Turell et al., 2012). The shape of the $\delta^{13}C$ curve across the LDE suggests a much slower rate of injection of ^{12}C to the ocean-atmosphere system than e.g. for the PETM; alternatively, the shape of the excursion might be also controlled by carbonate dissolution, as discussed for the PETM (e.g. McCarren et al., 2008). The onset of volcanism in the North Atlantic Igneous Province at the C27n / C26r polarity transition has been suggested as the causal trigger for the LDE (Dinarès-Turell et al., 2012).

Biotic and environmental effects of the LDE in open ocean, deep-sea sites are mainly based on studies of calcareous plankton (other than isotope analyses on benthic microfossils). These effects include the diversification of planktic foraminiferal communities in surface ocean habitats, the evolution of photosymbiotic lineages (Quillévéré and Norris, 2003) and the radiation of the nannofossil "fasciculiths group" *(Diantholitha* and *Lithoptychius)*, and point to an enhanced nutrient supply, warming and increased stratification of the upper water masses (Monechi et al., 2013; Jehle et al., 2015). In contrast, detailed studies on the seafloor conditions (based on benthic assemblages) are missing from the western Tethys, and few analyses have been carried out in other regions. The benthic foraminiferal turnover across the late Danian (including the D/S transition) was only described at a very low resolution in the Zumaia section (Schmitz et al., 1998, 2011; Alegret and Ortiz, 2010), where the boundary stratotype for the base of the Selandian Stage (i.e., the Danian/Selandian boundary) was defined, but no detailed studies have been published from this section, nor from other deep-water sections from the Tethys area. To our knowledge, the only studies dealing with benthic foraminiferal assemblages are based on shallower, shelf to upper bathyal sections from the Southern Tethys (Egypt and Tunisia; e.g. Sprong et al., 2012, 2013). In Egyptian sections, the LDE is placed at the base of an organic-rich dark bed (formerly thought to mark the D/S boundary) that contains a characteristic benthic foraminiferal assemblage with common *Neoeponides duwi* (Speijer and Schmitz, 1998; Speijer, 2003; Guasti et al., 2005; Alegret and Ortiz, 2013), a shallow-water (inner neritic) species. This assemblage, however, has not been recognized in other neritic sections from the Southern Tethyan margin (Guasti et al., 2006). The LDE sequence is condensed and represented by hiatus in the Tunisian sections, where it corresponds to a glauconite-rich indurated marl bed (Sprong et al., 2013). The assemblage turnover in both regions indicates shallowing associated with a sea-level lowering around the planktonic foraminiferal zones P3a-P3b transition, and more eutrophic conditions at the seafloor (Sprong et al., 2013).

Here we identify for the first time the LDE in a deep-water setting from the western Tethys (Caravaca section, Southern Spain), describe the calcareous nannofossil and benthic foraminiferal turnover across the late Danian, and infer the paleoenvironmental changes based on faunal and geochemical data.

2. Material and methods

Upper Danian sediments are well exposed along the Gredero ravine 4 km south of Caravaca de la Cruz (Murcia, S Spain; Fig. 1), which is located in the Subbetic Zone of the Betic Cordilleras. The studied sediments belong to the upper part of the Quipar-Jorquera Formation (Upper Cretaceous to Eocene; Vera, 1983) and they consist of grey marls and calcareous marls rich in foraminifera, with intercalations of pink or reddish marls across the upper Danian and lower Selandian (Molina, 1994; Arenillas and Molina, 1997). A total of 25 samples were collected along a 17 m thick sequence for micropaleontological studies (Fig. 2).

In order to analyse benthic foraminifera, samples were disaggregated in H_2O_2, washed over a 63 μm sieve and dried at <50 °C. The quantitative analysis is based on the study of approximately 300 benthic foraminifera picked from the >100 μm residue. A total of 141 species and 74 genera were identified (Table 1, Plate 1). All specimens were

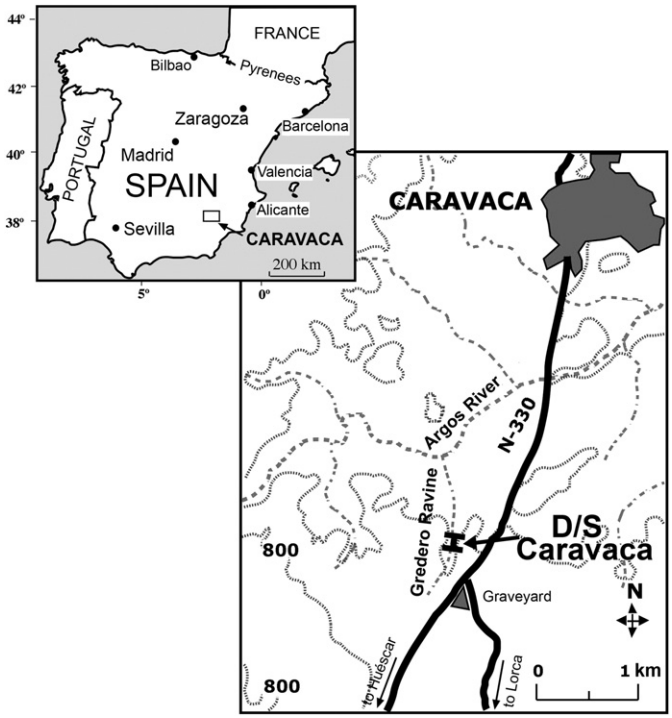

Fig. 1. Location of the Caravaca section (38° 04′ N, 01° 52′W) in Southern Spain.

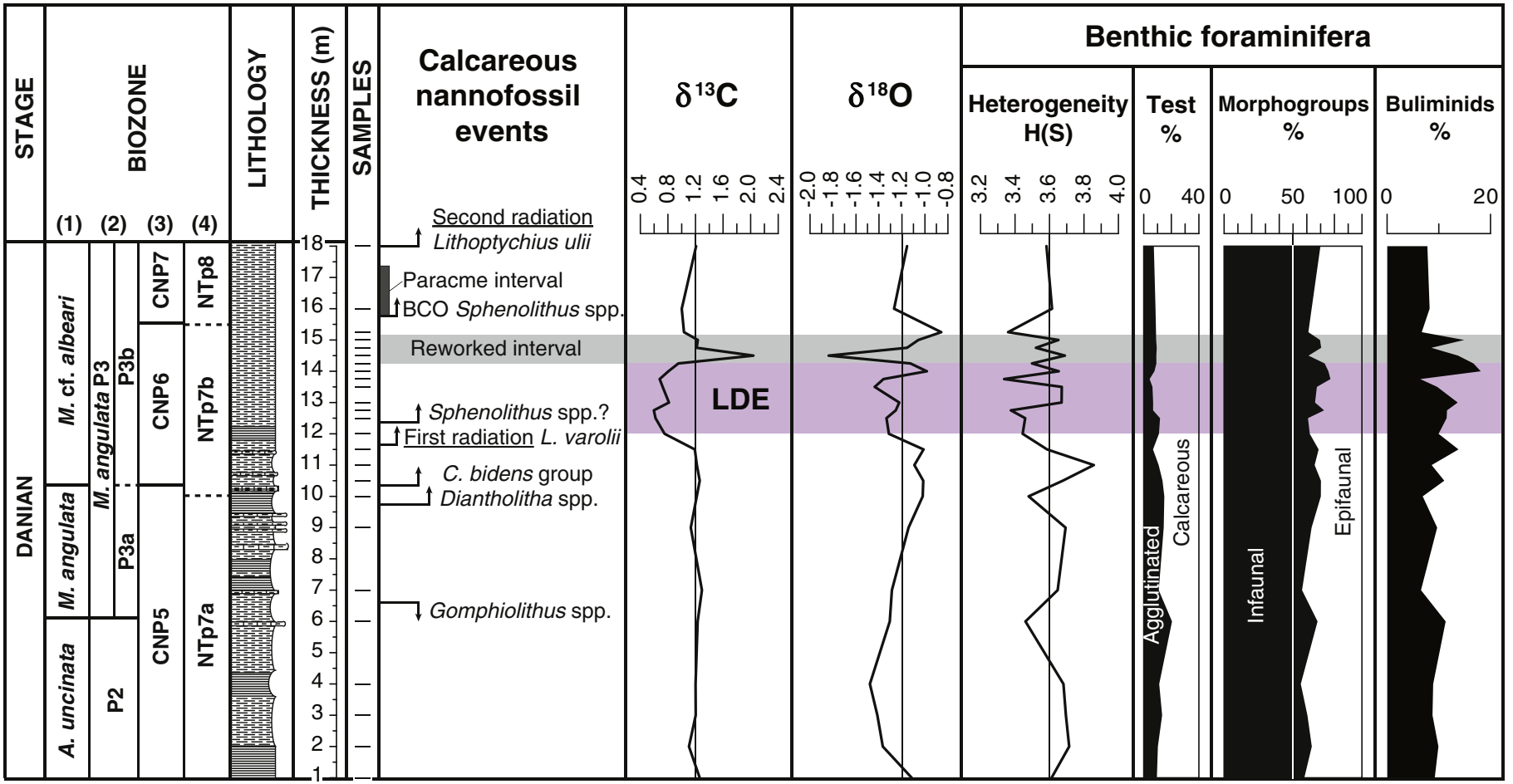

Fig. 2. Calcareous nannofossil events, benthic foraminiferal stable isotopes and indices across the Danian-Selandian transition at Caravaca. Shannon-Weaver heterogeneity index, percentage of agglutinated/calcareous tests, infaunal/epifaunal morphogroups and %buliminids. Planktic foraminiferal biozones (identified by Ortiz et al., 2008 and Arenillas, 2012) include (1) the *Acarinina uncinata*, *Morozovella angulata* and *Morozovella* cf. *albeari* biozones of Arenillas and Molina (1997), and (2) zones P2, P3a and P3b of Berggren and Pearson (2005). Calcareous nannofossil zones follow (3) Agnini et al. (2014) and (4) Varol (1989).

Table 1
Relative abundance of benthic foraminiferal taxa identified in the studied samples, and $\delta^{13}C$ and $\delta^{18}O$ values on *N. truempyi*.

	Samples																								
Species	1	2	3	4	6	7	9	10	10.5	11	11.5	12	12.5	12.75	13	13.5	13.75	14	14.25	14.5	14.75	15	15.25	16	18
Alabamina creta	0.7	0.0	0.0	0.0	0.0	0.4	0.7	0.4	0.4	0.7	0.7	0.0	0.0	0.0	0.3	0.7	0.0	0.0	0.0	1.1	0.0	0.3	0.0	0.0	0.9
Alabamina spp.	0.0	0.0	0.0	0.0	0.0	0.0	1.7	0.0	0.0	0.4	0.0	0.0	0.0	0.0	0.0	0.0	0.0	0.0	0.0	0.0	0.0	0.0	0.0	0.0	0.0
Alabamina wilcoxensis	0.0	0.0	0.0	0.0	0.0	0.0	0.0	0.0	0.0	0.0	0.0	0.0	0.0	0.0	0.0	0.0	0.0	0.0	0.0	0.0	0.9	0.0	0.0	0.3	0.0
Allomorphina velascoensis	0.0	0.0	0.0	0.5	0.0	0.0	0.0	0.0	0.0	0.0	0.0	0.0	0.0	0.0	0.0	0.0	0.0	0.0	0.0	0.0	0.4	0.0	0.0	0.0	0.0
Ammobaculites sp.	0.0	0.0	0.0	0.0	0.0	0.0	0.0	0.0	0.0	0.0	0.0	0.0	0.0	0.4	0.0	0.0	0.0	0.0	0.0	0.0	0.0	0.0	0.0	0.0	0.0
Ammodiscus sp.	0.0	0.0	0.0	0.0	0.0	0.0	0.0	0.4	0.0	0.0	0.0	0.4	0.3	0.0	0.0	0.0	0.0	0.0	0.0	0.0	0.0	0.0	0.0	1.0	0.0
Angulogavelinella avnimelechi	0.0	0.0	2.9	0.0	0.0	0.0	0.0	0.4	0.0	0.7	0.7	0.0	0.3	0.0	0.6	0.4	0.0	0.4	0.8	0.0	0.0	0.3	0.0	2.0	0.0
Anomalinoides acutus	0.3	0.0	0.0	0.0	0.4	0.0	0.0	0.0	0.0	0.0	0.4	0.0	1.0	0.0	0.0	0.7	0.0	0.4	0.0	0.0	0.0	0.0	0.0	0.0	0.0
Anomalinoides ammonoides	1.4	0.0	0.8	0.5	0.4	0.4	4.1	1.6	2.9	2.6	4.6	1.1	1.7	0.8	0.9	0.7	2.7	2.2	2.9	5.3	3.6	0.3	4.4	7.2	5.0
Anomalinoides cf. *ammonoides*	0.0	2.8	2.9	3.3	2.5	3.0	2.8	0.0	1.1	0.7	1.1	0.7	1.4	0.0	1.2	1.9	0.0	1.1	0.0	0.0	0.0	0.0	0.0	0.0	0.0
Anomalinoides praeacutus	0.0	0.0	0.0	0.5	0.0	0.0	0.0	0.0	0.0	0.0	0.0	0.0	0.0	1.2	0.0	0.0	0.0	0.0	0.4	0.4	0.0	0.0	0.0	0.3	0.5
Anomalinoides rubiginosus	0.0	0.0	0.0	0.0	0.0	0.0	0.0	0.0	0.0	0.0	0.0	0.0	0.0	0.0	0.0	0.0	0.0	0.0	0.0	0.0	0.0	0.0	0.0	0.0	0.5
Anomalinoides spp.	4.1	1.1	0.0	1.9	0.4	0.9	0.0	0.0	1.1	1.1	0.0	1.1	1.7	0.0	2.8	1.5	1.1	0.0	0.8	2.3	1.3	4.8	0.6	0.0	1.4
Aragonia aragonensis	0.7	0.0	0.4	0.0	0.0	0.0	0.0	0.0	0.0	0.4	0.0	0.0	3.4	0.0	4.3	1.5	0.0	3.0	4.2	0.4	0.4	0.0	0.6	0.3	0.5
Aragonia velascoensis	0.3	0.4	0.0	0.0	0.4	0.0	0.3	0.0	0.0	0.4	0.0	0.0	0.0	0.0	0.3	0.0	0.0	0.0	0.0	0.0	0.0	0.0	0.0	0.0	0.0
Arenobulimina truncata	0.0	0.0	0.0	0.0	0.0	0.0	0.0	0.0	0.0	0.0	0.0	0.0	0.0	0.0	0.0	0.0	0.0	0.0	0.4	0.0	0.0	0.0	0.0	0.3	0.0
Astacolus spp.	0.3	1.8	2.5	0.9	3.3	1.3	0.3	2.8	1.1	1.1	1.4	2.2	1.4	1.2	1.9	1.9	2.7	1.5	0.0	0.8	2.2	1.7	0.6	1.7	1.4
Bathysiphon spp.	0.7	0.0	1.3	0.0	1.3	0.4	0.7	0.8	0.4	0.0	0.0	0.0	0.3	0.8	0.0	0.0	0.0	0.0	0.8	0.0	0.4	0.3	1.1	0.0	0.0
Bolivinoides cf. *delicatulus*	0.0	0.0	0.0	0.0	0.4	0.0	0.0	0.0	0.0	0.0	0.0	0.4	0.0	0.0	0.0	0.0	0.0	0.0	0.0	0.0	0.0	0.3	0.0	0.0	0.0
Bolivinoides delicatulus	2.7	1.4	1.7	0.9	0.0	2.2	3.1	0.4	0.0	1.5	0.0	0.0	0.7	1.6	0.6	4.1	2.1	0.4	0.8	1.1	4.0	1.4	2.8	2.0	2.3
Bolivinoides sp. 1	0.0	0.7	0.0	0.5	0.0	0.4	0.0	0.4	0.4	0.0	0.0	0.4	0.0	0.0	0.0	0.0	0.0	0.0	0.0	0.0	0.0	0.0	0.6	0.0	0.0
Brizalina alata	0.0	0.0	0.8	0.0	0.0	0.0	0.0	0.4	0.0	0.0	0.0	0.0	0.0	0.0	0.0	0.0	0.0	0.0	0.0	0.0	0.0	0.0	0.0	0.0	0.0
Bulimina alazanensis	0.0	0.0	0.0	0.0	0.0	0.0	0.0	0.0	0.0	0.0	0.0	0.0	0.0	0.0	0.0	0.0	0.0	0.0	0.0	0.0	0.0	0.0	0.0	0.0	0.0
Bulimina kugleri	0.0	0.0	0.4	0.0	0.0	0.0	0.0	0.0	0.0	0.4	0.0	0.0	0.0	0.0	0.0	0.4	0.0	0.0	0.0	0.0	0.0	0.3	0.0	0.0	0.0
Bulimina midwayensis	0.0	0.0	0.0	0.0	0.0	0.0	0.0	0.0	0.0	0.0	0.0	0.0	0.0	0.0	0.0	0.0	0.0	0.0	0.0	0.0	0.0	0.0	0.0	0.7	0.0
Bulimina navarroensis	1.0	0.0	1.3	0.0	0.4	0.0	0.0	0.0	0.0	0.0	2.5	0.0	0.0	0.0	0.0	0.0	0.0	0.4	0.0	0.0	0.0	1.4	0.0	0.0	0.0
Bulimina paleocenica	0.0	0.0	0.0	0.0	0.0	0.0	0.0	0.0	0.0	0.0	0.0	0.0	0.0	0.0	0.0	0.0	0.0	0.0	0.0	0.0	0.0	0.0	0.6	0.0	0.0
Bulimina sp. 1	0.0	0.0	0.0	0.0	0.0	0.0	0.3	0.0	0.4	0.4	0.0	0.0	0.0	0.8	0.3	0.0	0.0	0.0	0.0	0.8	0.0	0.0	0.0	0.0	0.0
Bulimina sp. 2	0.7	0.7	0.0	0.5	0.0	0.0	2.4	0.0	2.9	1.1	2.5	0.4	0.0	1.6	1.2	1.1	2.7	2.2	2.5	1.5	0.9	1.7	0.6	0.3	1.4
Bulimina trinitatensis	3.7	7.4	2.9	4.7	7.5	2.2	3.8	4.4	5.1	4.1	2.8	5.9	3.4	3.6	4.6	5.6	2.1	7.7	4.6	8.4	4.9	7.6	3.9	5.5	3.2
Bulimina velascoensis	0.0	0.0	0.0	0.0	0.0	0.0	0.0	0.0	0.0	0.0	0.0	0.0	0.0	0.0	0.0	0.0	0.0	0.0	0.0	0.0	0.0	0.0	0.0	0.3	0.0
Bulimina sp. 3	0.0	0.0	0.0	0.0	0.0	0.0	0.3	0.0	0.4	0.0	0.7	0.0	0.0	0.0	0.0	0.0	0.0	0.0	0.0	0.0	0.0	1.0	0.0	0.0	0.0
Buliminella beaumonti	1.4	0.0	0.8	0.9	0.4	1.7	0.3	0.8	1.5	1.1	2.5	3.3	6.4	0.8	2.5	1.5	0.0	3.0	4.2	1.9	0.4	1.7	0.0	0.0	2.7
Buliminella grata	0.0	0.0	0.0	0.0	0.0	0.0	0.0	0.8	0.0	0.0	1.1	0.0	0.7	0.0	0.3	0.0	0.0	2.2	0.0	0.4	0.0	0.7	0.6	0.0	0.0
Cassidulina sp.	0.0	0.0	0.0	0.0	0.0	0.0	0.0	0.0	0.0	0.4	0.0	0.0	0.0	0.0	0.0	0.0	0.0	0.0	0.0	0.0	0.0	0.0	0.0	0.0	0.0
Cibicidoides cf. *mexicanus*	0.0	0.0	0.0	0.5	0.8	0.0	0.0	0.0	0.0	0.4	0.0	0.0	0.3	0.0	0.0	0.0	0.0	0.4	0.0	0.8	0.0	0.3	0.0	0.0	0.0
Cibicidoides cf. *pseudoperlucidus* (+ juv)	0.0	0.0	0.0	0.5	0.8	1.3	0.3	0.0	0.0	0.0	0.0	0.0	0.0	0.4	0.0	1.9	4.3	1.5	1.7	0.4	1.3	0.0	0.0	1.4	1.4
Cibicidoides dayi (+ juv)	0.0	0.7	0.0	0.9	0.0	0.9	0.0	0.4	0.0	1.1	0.0	0.4	0.0	0.0	0.3	0.4	0.0	1.1	1.7	0.4	0.0	0.0	0.0	0.0	0.0
Cibicidoides eocaenus	0.0	0.4	0.0	0.0	0.0	0.0	0.0	0.0	0.0	0.0	0.0	0.0	0.0	0.0	0.0	0.0	0.0	0.0	0.0	0.4	0.0	0.3	0.0	0.0	0.0
Cibicidoides howelli	2.7	2.8	4.6	1.9	1.3	0.9	2.8	2.0	1.5	0.0	1.8	1.5	2.7	0.8	0.9	2.2	0.0	0.7	1.3	2.3	0.9	1.7	1.7	0.0	1.4
Cibicidoides hyphalus	6.8	5.3	2.5	7.5	1.7	4.8	3.4	0.8	1.5	3.0	1.1	2.6	8.1	0.4	2.8	0.7	1.6	0.4	0.0	0.8	3.6	3.5	1.7	8.5	0.9
Cibicidoides sp. 1	0.7	0.0	0.0	0.5	0.0	0.0	0.0	0.4	0.0	0.0	0.0	0.0	0.0	0.0	0.0	0.4	0.0	0.0	0.0	0.8	1.3	0.0	0.0	0.0	0.0
Cibicidoides sp. 2	0.0	0.0	0.0	0.5	0.0	0.0	0.0	0.0	0.0	0.0	0.0	0.0	0.0	0.8	0.0	0.4	0.5	0.0	0.0	0.0	0.0	0.0	0.6	0.0	0.0
Cibicidoides velascoensis (+ juv)	1.7	0.4	1.7	0.9	0.8	0.0	0.0	2.4	0.0	0.4	0.0	0.0	0.7	0.0	0.6	0.4	0.0	1.1	0.0	0.0	0.0	0.7	0.6	0.7	0.9
Cibicidoides westi	0.0	0.0	0.0	0.0	0.0	0.0	0.0	0.0	0.0	0.0	0.0	0.0	0.0	0.8	0.0	0.0	1.1	0.0	0.0	0.0	0.0	0.0	0.0	0.0	0.0
Clavulinoides amorpha	0.3	0.0	0.0	0.0	1.7	0.4	0.0	1.2	0.4	0.4	0.0	0.4	0.0	0.0	0.0	0.4	0.0	0.4	0.8	0.4	0.4	0.0	0.0	0.0	1.8
Clavulinoides spp. (+ juv)	1.0	1.4	2.9	0.9	2.1	2.2	4.5	0.4	1.1	1.9	2.5	1.5	0.3	2.0	1.2	2.2	0.5	0.7	1.3	1.1	1.8	2.1	0.0	1.4	1.8
Clavulinoides trilatera	1.0	1.1	0.0	0.0	0.4	0.9	0.0	0.4	1.8	1.1	0.0	0.0	0.7	0.0	0.3	0.0	0.0	0.4	0.0	0.4	0.4	0.0	0.0	0.0	0.5
Coryphostoma midwayensis	1.7	1.1	2.5	0.9	0.0	1.3	4.1	3.2	2.2	2.6	2.5	5.9	2.4	7.6	4.3	4.1	6.4	2.6	3.3	2.7	3.1	3.1	0.0	2.0	2.3
Dorothia bulleta/cylindracea	0.7	0.7	0.4	0.5	0.0	0.0	0.0	1.2	0.0	0.7	0.0	0.0	0.0	0.0	0.0	0.4	0.0	0.0	0.0	0.0	0.0	0.0	0.0	0.0	0.0
Dorothia crassa	0.3	1.4	1.3	0.9	3.3	0.0	0.3	0.8	0.0	0.4	0.4	0.4	0.7	0.0	0.0	0.0	0.0	0.7	1.7	1.9	0.0	0.3	1.7	1.0	1.4
Dorothia pupa	1.0	0.0	0.0	0.5	0.0	0.0	0.0	0.0	0.7	0.0	0.0	0.0	0.0	0.0	0.3	0.0	0.0	0.0	0.0	0.0	1.3	0.0	1.1	0.0	0.5
Ellipsoglandulina sp.	0.0	0.0	0.0	0.0	0.0	0.0	0.0	0.0	0.0	0.0	0.0	0.0	0.0	0.0	0.0	0.0	0.0	0.0	0.0	0.0	0.0	0.0	0.0	0.3	0.5
Eouvigerina spp.	0.0	0.0	0.0	0.0	0.0	0.0	0.0	0.0	0.0	0.0	0.0	0.0	0.0	0.8	0.0	0.0	2.1	0.0	0.0	0.0	0.0	0.0	0.0	0.0	4.1

Fissurina spp.	0.0	0.0	0.0	0.9	0.0	0.4	0.0	0.0	0.4	0.4	0.4	0.7	0.0	0.4	0.0	0.0	1.1	0.0	1.7	0.0	1.8	0.3	0.0	1.0	0.0
Gaudryina cf. *pyramidata*	0.0	0.0	0.0	0.0	0.0	0.4	0.0	0.0	0.0	0.0	0.0	0.0	0.0	0.0	0.0	0.0	0.0	0.0	0.0	0.4	0.0	0.0	0.0	0.0	0.0
Gaudryina pyramidata	0.0	0.0	1.7	1.4	1.3	0.4	0.3	0.0	0.0	0.0	0.7	0.4	0.0	0.0	0.0	0.0	0.0	0.0	0.4	0.4	2.2	0.3	0.0	1.7	0.0
Gaudryina sp. 1	1.0	1.1	0.8	0.0	0.8	0.9	0.0	0.0	0.0	0.4	0.4	0.0	0.3	0.0	0.0	0.4	0.0	0.0	0.0	0.4	0.0	0.0	0.0	0.0	0.0
Gaudryina sp. 2	0.0	0.4	0.8	0.0	0.0	0.0	0.0	0.0	0.0	0.0	0.4	0.0	0.0	0.0	0.0	0.4	0.0	0.0	0.0	0.0	0.0	0.0	0.0	0.0	0.0
Gaudryina sp. 3	0.0	0.0	0.0	0.5	0.0	0.0	0.0	0.0	0.0	0.0	0.0	0.0	0.0	0.0	0.0	0.0	0.0	0.4	0.0	0.0	0.0	0.0	0.0	0.0	0.5
Gaudryina spp.	0.0	0.0	0.0	0.0	0.0	0.0	0.0	3.6	0.0	0.0	0.0	0.0	0.0	0.0	0.0	0.0	0.0	0.0	0.4	0.0	0.4	0.0	0.6	0.0	0.0
Globocassidulina subglobosa	0.0	0.0	0.0	0.0	0.0	0.4	0.0	0.0	0.4	0.0	0.7	0.0	0.0	0.0	0.3	0.0	0.0	0.4	0.0	0.0	0.0	0.0	0.0	0.0	0.0
Globorotalites spp.	0.7	0.4	0.8	0.9	0.0	3.0	0.0	0.0	0.4	0.4	0.4	0.7	1.4	1.2	0.3	0.4	0.0	0.0	0.8	0.0	0.0	0.0	0.0	1.7	2.3
Globulina sp.	0.0	0.0	0.0	0.0	0.0	0.0	0.0	0.0	0.0	0.0	0.0	0.0	0.0	1.6	0.0	0.0	0.0	0.0	0.4	0.0	0.0	0.0	0.6	0.7	0.9
Glomospira sp.	0.0	0.0	0.0	0.0	0.0	0.0	0.0	0.0	0.0	0.0	0.0	0.0	0.0	0.4	0.0	0.0	0.0	0.0	0.0	0.0	0.0	0.0	0.0	0.0	0.0
Guttulina spp.	0.0	0.4	0.0	0.0	0.0	0.0	0.0	0.4	0.7	0.0	0.4	0.0	0.0	0.4	0.3	0.0	1.6	0.4	0.0	0.4	0.0	0.0	1.1	0.0	0.0
Gyroidinoides acutus	0.0	0.0	0.0	0.0	0.4	0.0	0.0	0.0	0.4	0.0	0.7	0.0	0.7	0.0	0.6	0.4	0.0	0.0	0.0	0.4	0.0	0.0	0.0	0.0	0.0
Gyroidinoides angulosa	0.0	0.0	0.0	0.0	1.3	0.0	0.0	0.0	0.0	0.0	0.0	0.0	0.0	0.0	0.0	0.0	0.0	0.0	0.0	0.0	0.0	0.0	0.0	0.0	0.0
Gyroidinoides beisseli	0.3	1.4	3.3	1.9	0.8	0.4	0.0	0.0	0.0	0.0	0.0	0.7	1.6	0.6	0.0	1.1	1.5	1.3	0.8	1.8	0.3	2.8	2.0	0.5
Gyroidinoides sp. 1	0.3	1.8	1.7	1.9	0.8	0.4	1.4	1.2	0.0	2.2	0.7	0.4	1.0	0.0	0.6	0.4	0.0	0.7	0.0	0.0	0.0	1.0	0.0	0.0	0.0
Gyroidinoides depressus	0.7	0.4	0.4	0.0	0.8	0.0	0.3	1.2	0.0	0.4	0.0	0.4	0.0	0.8	0.3	0.4	0.0	0.7	0.8	0.0	0.4	0.3	0.0	0.0	0.5
Gyroidinoides girardanus	1.0	2.5	2.9	0.9	0.4	0.0	0.0	0.0	0.4	1.1	0.7	1.8	0.3	0.8	2.2	1.5	0.0	1.5	2.1	1.1	0.9	1.4	0.6	0.7	1.4
Gyroidinoides globosus	1.4	0.4	2.1	1.4	0.8	0.0	0.3	2.0	0.4	1.1	1.1	1.5	0.7	0.0	1.2	0.7	2.1	0.7	0.0	0.4	1.8	1.4	2.2	0.7	0.5
Gyroidinoides planulatus	0.0	0.4	0.0	0.0	0.0	0.9	0.0	0.0	0.4	0.4	0.0	0.0	0.0	0.0	0.3	0.4	0.0	0.4	0.0	0.0	0.0	0.0	0.0	0.0	0.9
Gyroidinoides spp.	0.0	0.0	0.0	0.0	0.0	0.9	0.0	0.0	1.1	1.1	0.0	0.4	0.0	0.4	0.0	0.4	0.5	0.0	0.0	0.4	0.0	0.7	1.7	0.3	0.5
Gyroidinoides subacutus	0.0	0.0	0.0	0.0	0.0	0.0	0.0	0.0	0.4	0.0	0.0	0.0	0.0	0.0	0.0	0.0	0.0	0.0	0.0	0.0	0.0	1.4	0.0	0.0	0.0
Haplophragmoides spp.	0.3	0.7	0.8	0.0	0.8	0.0	0.0	0.4	0.0	0.0	0.0	0.0	0.0	0.0	0.3	0.0	0.0	0.0	0.0	0.0	0.0	1.0	0.0	0.0	0.0
Hemirobulina spp.	1.0	0.0	0.0	0.5	0.0	0.4	0.3	0.0	0.4	0.4	1.4	0.0	0.3	0.0	0.3	0.7	0.0	0.4	0.0	0.4	0.0	0.7	0.0	0.0	0.0
Karreriella spp.	0.0	0.0	0.0	0.5	0.0	0.0	0.0	0.0	0.0	0.0	0.0	0.0	0.0	0.0	0.0	0.0	0.0	0.0	0.0	0.0	0.0	0.0	0.0	0.0	0.0
Laevidentalinids	2.7	1.4	4.2	1.9	4.6	1.3	3.4	0.0	8.5	4.9	1.8	5.1	6.4	8.8	3.1	2.2	8.5	2.2	7.5	3.4	6.3	4.8	5.6	6.1	6.4
Lagena spp.	8.8	5.7	4.6	6.1	8.4	7.4	7.2	14.1	10.3	7.1	11.7	6.6	2.7	3.6	5.6	7.1	5.3	8.1	1.7	6.5	3.1	4.5	5.0	2.4	4.1
Lenticulina spp.	3.4	4.2	5.4	2.8	2.5	2.6	3.1	7.7	3.7	4.1	6.7	4.8	3.7	5.2	3.4	5.6	4.8	5.5	6.3	5.3	4.5	5.2	7.2	4.8	6.4
Marssonella floridana	0.0	0.0	1.3	0.0	0.0	0.0	0.0	0.8	0.0	0.4	0.0	0.0	0.0	0.0	0.0	0.7	0.0	0.4	0.0	0.4	0.4	0.3	0.0	0.3	0.5
Marssonella oxycona	0.3	0.7	0.8	1.4	0.8	1.7	0.0	0.0	0.7	0.4	0.4	0.0	0.0	0.0	0.6	0.4	0.0	0.4	0.4	0.8	0.0	0.3	0.0	0.7	0.0
Marssonella spp.	0.0	0.0	0.0	0.0	0.0	0.0	0.0	0.0	0.0	0.7	0.0	0.0	0.3	0.0	0.0	0.0	0.0	0.0	1.3	0.4	0.0	0.0	1.1	0.3	0.0
Neoflabellina cf. *jarvisi*	0.0	0.0	0.0	0.0	0.0	0.0	0.0	0.0	0.0	0.0	0.0	0.0	0.0	0.0	0.0	0.0	0.0	0.0	0.0	0.0	0.0	0.0	1.1	0.0	0.0
Neoflabellina jarvisi (+ juv)	0.0	0.4	0.0	0.5	0.0	0.4	0.3	0.4	0.7	0.4	0.0	0.0	0.7	0.0	0.0	0.0	0.0	0.7	0.0	0.4	0.0	0.0	0.0	0.0	0.0
Nodosarella spp.	0.0	0.0	0.0	0.0	0.4	0.4	0.0	0.0	0.0	0.4	0.0	0.0	0.0	0.0	0.0	0.0	0.0	0.0	0.0	0.0	0.0	0.0	0.0	0.0	0.0
Nonion havanense	1.0	2.1	0.0	0.9	0.4	0.0	0.0	1.2	1.1	1.5	2.5	1.5	1.0	4.0	3.4	3.0	4.8	1.8	3.8	0.4	1.8	2.1	0.0	3.8	3.7
Nonion sp. 1	0.0	1.8	0.0	0.0	0.0	1.3	0.7	4.8	0.7	0.4	2.5	1.5	0.3	0.0	0.9	1.1	0.0	1.8	0.0	1.9	0.0	1.7	0.0	0.0	0.0
Nonion spp.	1.7	0.0	0.0	0.5	0.0	0.0	0.0	0.0	0.0	1.1	0.0	0.0	0.0	0.0	0.3	0.0	0.0	0.0	0.0	0.0	0.0	0.0	0.0	0.0	0.0
Nonionella spp.	0.0	0.0	0.0	0.5	0.0	0.4	0.0	0.8	0.0	0.0	0.4	0.0	0.7	0.0	0.0	1.9	1.1	0.0	0.0	1.1	0.0	1.0	0.0	0.0	0.0
Nuttallides truempyi	11.1	5.7	9.2	9.3	16.7	14.8	6.6	11.3	5.9	7.5	9.5	16.5	14.5	12.4	12.4	6.7	9.0	9.6	10.4	11.0	7.2	9.3	12.2	6.5	8.2
Nuttallinella florealis	0.7	0.0	0.0	0.0	0.0	1.3	3.1	0.8	1.8	1.9	2.8	1.1	0.0	0.0	2.5	2.6	0.0	0.0	0.4	3.8	1.3	1.0	1.7	0.0	0.0
Nuttallinella spp.	0.0	0.7	0.0	1.9	0.0	1.3	0.0	0.0	0.0	0.0	0.0	0.0	0.0	2.4	0.0	0.0	1.1	0.0	0.0	0.0	0.0	0.3	3.3	4.1	0.9
Oolina spp.	0.0	0.0	0.0	0.0	0.0	0.0	0.0	0.0	0.0	0.0	0.0	0.0	0.0	0.4	0.0	0.0	0.0	0.0	1.3	0.0	0.0	0.0	0.0	0.0	2.3
Oridorsalis plummerae	3.4	0.4	0.8	0.5	0.4	0.9	0.0	0.0	0.4	0.0	0.0	0.4	0.3	0.0	0.0	0.0	0.0	0.7	0.0	0.4	0.0	0.0	0.0	0.0	0.0
Oridorsalis umbonatus	0.0	1.4	2.5	1.9	1.3	2.2	3.8	2.8	1.8	2.6	3.9	2.2	2.0	2.0	1.2	2.2	3.2	3.3	1.7	3.0	2.2	1.4	5.6	2.4	0.0
Osangularia sp. 1	0.0	0.0	0.0	0.0	0.0	0.0	0.3	0.0	0.0	0.0	0.4	0.0	0.3	0.0	0.3	0.0	0.0	0.0	0.0	0.0	0.0	0.0	0.0	0.0	0.0
Osangularia sp. 2	0.0	0.0	0.0	0.0	0.0	0.0	0.0	0.0	0.0	0.0	0.4	0.7	0.0	0.0	0.0	0.0	0.0	0.0	0.0	0.4	0.0	0.3	0.0	0.0	0.0
Osangularia spp.	0.3	1.8	0.4	0.5	0.4	4.3	3.4	0.8	1.5	0.4	1.4	0.4	0.0	0.4	0.6	0.4	0.0	0.0	0.4	1.1	1.8	0.7	2.2	0.0	0.5
Osangularia velascoensis	0.0	0.0	0.4	0.0	0.0	0.0	0.0	0.0	0.7	0.4	0.0	0.0	0.0	0.0	0.0	0.0	0.0	0.0	0.0	0.0	0.0	0.0	0.0	0.3	0.0
Osangularia sp. 4	0.0	0.0	0.0	0.0	0.0	0.0	0.0	0.0	0.0	0.4	0.0	0.4	0.0	0.0	0.0	0.0	0.0	0.0	0.0	0.0	0.0	0.0	0.0	0.0	0.0
Palliolatella spp.	2.4	0.7	0.0	0.9	0.8	0.4	0.3	0.4	0.0	0.0	0.0	0.0	0.0	0.0	0.3	0.4	0.0	0.0	0.0	0.4	0.0	0.0	0.6	0.3	0.0
Osangularia sp. 3	2.0	4.2	2.9	5.6	0.0	0.4	1.0	2.0	4.4	4.5	0.4	4.0	0.0	0.0	0.3	0.0	0.0	0.0	0.0	3.0	0.0	0.0	0.0	0.0	0.0
Paralabammina hilldebrandti	2.4	2.8	0.8	2.8	0.0	0.4	0.7	0.8	2.2	1.5	2.8	1.1	0.3	1.6	2.2	6.3	0.5	0.0	1.3	1.5	4.0	1.0	5.6	0.0	1.4
Planulina sp.	0.3	0.0	0.0	0.0	0.0	0.0	0.0	0.0	0.0	0.0	0.0	0.0	0.0	0.0	0.0	0.0	0.0	0.0	0.0	0.0	0.0	0.0	0.0	0.0	0.0
Pleurostomella spp.	0.3	0.7	0.0	0.0	0.0	0.0	0.0	0.0	1.1	0.4	0.7	0.0	0.0	1.6	0.0	0.0	1.6	0.0	0.8	0.8	2.2	0.3	1.1	1.0	1.8
Polimorphinids	1.7	3.5	3.3	2.3	0.8	5.2	2.4	2.4	4.0	4.1	1.4	2.2	3.7	7.2	1.9	4.5	5.9	6.3	4.6	1.5	9.0	5.5	6.1	2.7	3.2
Praebulimina sp.	0.0	0.0	0.0	0.0	0.0	0.0	0.0	0.0	0.0	0.0	0.0	0.0	0.0	0.0	0.0	0.0	0.5	0.0	0.8	0.0	0.0	0.0	0.0	0.3	0.5
Pseudoclavulina trinitatensis	0.0	0.0	0.0	0.0	0.0	0.0	0.0	0.0	0.0	0.0	0.0	0.4	0.7	0.0	0.0	0.0	0.0	0.0	0.0	0.0	0.0	0.0	0.0	0.0	0.0
Pseudouvigerina plummerae	0.0	0.0	0.0	0.0	0.0	0.0	0.0	0.0	0.0	0.0	0.0	0.0	0.0	0.0	0.0	0.0	0.0	0.0	0.0	0.0	0.0	0.0	0.0	0.3	0.0
Pullenia coryelli	0.0	0.0	0.0	0.0	0.0	0.4	0.0	0.8	0.4	0.0	0.4	0.0	0.0	0.0	0.0	0.0	0.0	0.0	0.0	0.0	0.0	0.0	0.0	0.0	0.0

(continued on next page)

Table 1 (*continued*)

Species	Samples																								
	1	2	3	4	6	7	9	10	10.5	11	11.5	12	12.5	12.75	13	13.5	13.75	14	14.25	14.5	14.75	15	15.25	16	18
Pullenia cretacea	0.0	0.0	0.0	0.0	0.0	0.0	0.3	2.8	0.7	0.4	0.4	0.0	0.3	0.4	0.0	1.1	0.0	0.4	1.3	0.4	0.4	0.3	1.1	2.4	1.8
Pullenia jarvisi	0.7	0.0	0.0	0.0	1.7	1.3	1.0	0.4	0.4	0.4	1.8	0.7	1.0	0.8	1.9	0.0	2.7	0.7	1.3	0.4	1.3	0.0	1.1	1.4	0.5
Pullenia quinqueloba	0.7	0.7	0.0	0.0	0.0	0.0	0.3	0.0	0.4	0.0	0.0	0.0	0.0	0.0	0.6	0.0	0.0	1.5	0.0	0.0	0.0	0.0	0.0	0.0	0.0
Pullenia spp.	0.3	0.7	0.8	1.9	0.4	2.6	0.7	0.0	1.1	1.9	0.0	1.5	0.7	0.0	0.3	1.1	0.0	0.0	0.0	1.5	0.0	1.4	0.0	1.7	0.5
Pyramidina rudita	1.4	0.0	0.8	0.5	1.3	0.4	0.7	0.0	0.4	1.1	0.7	0.0	0.0	0.0	2.2	0.0	0.0	1.8	0.0	0.4	0.0	0.3	0.0	0.0	0.0
Pyrulinoides spp.	0.0	3.2	1.3	0.5	3.8	0.0	2.8	0.0	1.5	1.1	0.0	0.4	1.4	0.0	2.2	1.1	0.0	1.5	0.0	0.0	0.0	1.4	0.0	1.4	0.5
Quadratobuliminella pyramidalis	1.0	1.8	2.5	2.3	1.3	1.3	1.0	0.8	0.4	0.4	1.1	0.4	1.0	4.8	2.5	1.1	1.1	0.7	4.6	0.4	2.2	0.0	1.1	1.0	0.0
Quadrimorphina allomorphinoides	1.7	0.4	2.1	0.5	0.8	0.4	1.0	0.0	1.1	0.0	0.4	0.0	0.3	1.2	0.0	0.4	2.1	1.1	5.0	1.1	1.3	1.0	0.0	0.0	0.5
Quadrimorphina cf. *allomorphinoides*	1.0	0.7	0.0	0.0	0.0	0.9	0.0	0.0	0.0	0.7	1.1	2.6	0.0	0.0	4.0	3.7	0.0	1.5	0.0	0.0	0.0	0.0	0.0	2.0	0.0
Quadrimorphina profunda	0.0	0.0	0.0	0.0	0.0	0.0	0.0	0.0	0.0	0.0	0.0	0.0	0.0	0.0	0.0	0.0	0.0	0.0	0.0	0.0	0.0	0.0	0.0	0.0	0.0
Recurvoides spp.	0.0	0.0	0.0	0.5	0.0	0.0	0.0	0.0	0.0	0.0	0.0	0.0	0.0	0.4	0.0	0.0	0.0	0.0	0.0	0.0	0.0	0.0	0.0	0.0	0.0
Remesella varians (+ juv)	0.3	0.0	0.0	0.0	0.0	0.0	0.0	0.8	0.7	0.4	0.0	0.0	0.0	0.0	0.3	0.4	0.0	1.1	0.0	0.0	0.0	0.0	0.0	0.0	0.0
Repmanina charoides	0.0	0.4	0.4	0.0	0.4	0.0	0.7	0.0	0.4	0.4	0.0	0.0	0.0	0.0	0.0	0.4	0.0	0.0	0.0	0.4	0.4	0.0	0.0	0.3	0.0
Saracenaria spp.	0.7	0.7	0.0	0.0	0.4	1.3	0.7	0.4	1.8	0.7	0.0	0.4	1.0	0.0	0.0	0.0	0.0	1.1	0.0	0.8	0.0	1.0	0.0	0.0	0.0
Siphonodosaria sp.	0.0	0.0	0.0	0.0	0.0	0.0	0.0	0.0	0.0	0.0	0.4	0.0	0.0	0.0	1.9	0.0	0.0	0.0	0.4	0.0	0.9	0.0	0.0	2.4	0.9
Sitella spp.	0.0	0.0	0.0	0.0	0.4	0.9	0.3	0.0	0.0	0.0	0.0	0.0	0.0	0.0	0.0	0.0	0.0	0.0	0.0	0.0	0.0	0.0	0.0	0.0	0.0
Spiroplectammina spectabilis (+ juv)	2.4	2.5	0.8	4.2	7.1	3.5	7.9	4.0	7.4	3.7	2.1	7.7	8.1	2.8	3.7	0.7	3.7	3.3	1.3	2.3	1.3	4.2	3.3	1.0	0.5
Stensioina beccariiformis	2.7	7.4	0.0	6.5	4.6	4.3	2.8	1.2	1.8	4.9	4.6	0.4	3.4	3.6	0.3	3.3	4.8	2.2	1.3	2.7	4.5	4.5	2.2	2.0	8.7
Stilostomella spp.	0.0	1.1	2.1	0.5	0.8	0.0	1.0	0.0	0.0	1.9	0.0	0.4	0.0	2.0	0.0	0.0	2.1	0.0	0.0	0.4	0.0	0.0	0.0	0.0	0.0
Tappanina selmensis	0.7	0.0	0.4	0.0	0.0	0.0	0.3	0.0	0.0	0.0	0.0	0.4	0.0	0.0	0.0	0.0	0.5	0.0	0.0	0.4	0.0	0.3	0.0	0.3	0.9
Trochammina sp.	0.0	0.0	0.0	0.0	0.0	0.0	0.0	0.0	0.0	0.0	0.0	0.0	0.0	0.0	0.0	0.0	0.0	0.0	0.4	0.0	0.0	0.0	0.0	0.3	0.0
Turrilina sp.	0.0	0.0	0.0	0.0	0.0	0.0	0.3	0.0	0.0	0.0	0.0	0.0	0.0	0.0	0.0	0.0	0.0	0.0	0.0	0.0	0.0	0.0	0.0	0.0	0.0
Valvalabamina lenticula	0.0	1.1	0.8	0.0	0.0	0.9	1.7	0.8	0.0	0.0	0.4	0.4	0.0	0.8	0.9	0.4	0.5	0.0	0.0	0.0	0.0	0.0	0.0	0.7	0.9
Valvalabamina spp.	0.0	0.4	0.0	0.0	0.0	0.0	0.0	0.0	0.0	0.0	0.7	1.5	1.0	0.0	0.0	0.0	0.0	0.7	0.0	0.0	0.0	0.0	0.0	0.0	0.0
Valvulineria spp.	0.3	0.0	1.3	0.0	0.0	0.4	0.3	0.8	0.0	0.4	0.0	0.0	0.0	0.0	0.0	0.0	0.0	0.0	0.0	0.0	0.0	0.0	0.0	0.0	0.0
Virgulopsoides sp.	1.0	0.0	0.0	0.0	0.0	0.0	0.0	0.0	0.0	0.0	0.0	0.0	0.0	0.0	0.0	0.0	0.0	0.0	0.0	0.0	0.0	0.0	0.0	0.0	0.0
Vulvulina sp. (juv)	0.0	0.0	0.0	0.0	0.4	0.0	0.0	0.0	0.0	0.0	0.0	0.0	0.0	0.0	0.0	0.0	0.0	0.0	0.0	0.0	0.0	0.0	0.0	0.0	0.0
Total	100	100	100	100	100	100	100	100	100	100	100	100	100	100	100	100	100	100	100	100	100	100	100	100	100
Agglutinated	9.5	10.2	13.3	11.2	20.5	10.9	14.5	14.9	13.6	10.8	6.7	11.0	11.8	6.8	6.8	6.3	4.3	7.7	9.2	9.1	9.4	9.0	8.9	8.5	7.3
Calcareous	90.5	89.8	86.7	88.8	79.5	89.1	85.5	85.1	86.4	89.2	93.3	89.0	88.2	93.2	93.2	93.7	95.7	92.3	90.8	90.9	90.6	91.0	91.1	91.5	92.7
Epifaunal	42.2	36.4	39.6	44.4	32.2	43.5	36.6	29.8	29.8	34.3	31.4	37.9	39.2	27.5	34.1	32.7	22.9	24.4	27.1	38.8	29.6	30.4	38.9	36.5	30.1
Infaunal	57.8	63.6	60.4	55.6	67.8	56.5	63.4	70.2	70.2	65.7	68.6	62.1	60.8	72.5	65.9	67.3	77.1	75.6	72.9	61.2	70.4	69.6	61.11	63.5	69.9
δ13C VPDB (*N. truempyi*)	1.26	1.11	1.20	1.20	1.23	1.29	1.13	1.22	1.26	1.22	1.19	0.75	0.62	0.60	0.81	0.72	0.68	0.81	0.95	2.04	1.22	1.23	1.03	1.00	1.21
δ18O VPDB (*N. truempyi*)	−1.11	−1.37	−1.41	−1.48	−1.31	−1.29	−1.14	−1.02	−1.01	−1.09	−1.01	−1.31	−1.33	−1.25	−1.22	−1.44	−1.36	−0.98	−1.13	−1.84	−1.16	−1.06	−0.86	−1.27	−1.16

mounted on microslides for identification at species and genus level, following Tjalsma and Lohmann (1983), van Morkhoven et al. (1986), Loeblich and Tappan (1987) and Alegret and Thomas (2001). We calculated the relative abundances of species (Table 1), and the H (S) or Shannon Weaver index as a proxy for the heterogeneity of the assemblages (Fig. 2). The calcareous-agglutinated and the infaunal-epifaunal ratios were assessed (Fig. 2), the latter based on morphotypic analysis (e.g. Corliss and Chen, 1988) and serving as a proxy for combined oxygenation and food availability in the deep sea (Jorissen et al., 2007).

R-mode (species) hierarchical cluster analyses were performed to identify groups of benthic foraminiferal species with similar distribution patterns. The unweighted pair-group average algorithm (UPGMA) and the Pearson correlation, as similarity coefficient, were used. For this analysis we constructed a dataset of species with a relative abundance >3% in at least one sample, excluding rare (1–2%) and very rare taxa (<1%). Juvenile forms were included in counts of adult forms of the same species. A total of 53 species (48 calcareous and 5 agglutinated) and 25 samples were used in the cluster analysis. As an attempt to identify the environmental variables that may have controlled the distribution pattern of benthic foraminifera, Detrended Correspondence Analysis (DCA) in both R-mode and Q-mode were performed on the same dataset. Statistical analyses were made using PAST software (Hammer et al., 2001).

Calcareous nannofossils were examined on smear-slides prepared following standard methods and analysed under cross-polarised and plain light using a Zeiss Axioplan2 petrographic microscope at 1250× magnification. In this study mainly qualitative analyses were performed in order to define the biostratigraphy and to allow the identification of the marker bioevents (Fig. 2). Since the Danian-Selandian transition is characterised by the appearance of "fasciculiths" (*Diantholitha*, *Lithoptychius*, *Fasciculithus*) and *Sphenolithus*, and these taxa are very rare in the lower part of their range, calcareous nannofossil analyses were carried out on two tracks of the smear slide in order to detect the index species. Species concepts largely follow Perch-Nielsen (1985) and for the "fasciculiths group" we refer to Monechi et al. (2012, 2013 and references therein).

The geochemical analyses were carried out at the Stable Isotope Laboratory of the Swiss Federal Institute of Technology Zurich (ETH). Twenty-five samples were prepared for stable isotope analysis by extracting *Nuttallides truempyi* specimens from each level. Samples were analysed on a Finnigan GasBench II carbonate device connected to a ThermoFisher Delta V PLUS mass spectrometer. The reproducibility of the measurements based on replicated standards was ±0.04‰ for $\delta^{13}C$ and ±0.05‰ for $\delta^{18}O$. The instrument is calibrated with the international standards NBS19 and NBS18. The obtained results are shown in Fig. 2, the isotope values being reported in the conventional delta notation with respect to VPDB. Oxygen isotope values are prone to diagenetic alteration during burial and they were not used for paleotemperature estimations but only to assess the degree of diagenetic overprinting on the $\delta^{13}C$ record.

3. Results

3.1. Stable isotopes

Results of mono-specific isotope analyses on benthic foraminifera (*Nuttallides truempyi*) show pretty stable $\delta^{13}C$ values in the lower half of the Caravaca section (from 1 to 11.5 m), with positive values ranging close to 1.2‰. The $\delta^{13}C$ record shows a shift to less positive values in an interval from 12 to 14.25 m, where values range from 0.6 to 0.9‰ and display a ~0.6 per mille carbon isotope excursion (CIE), showing the lowest values recorded in the studied section. The $\delta^{13}C$ record returns to more positive values immediately above the CIE, across an anomalous interval (samples 14.5 to 15.25 m), hereafter called "interval R" (reworked interval in Fig. 2), with $\delta^{13}C$ values of 2.0‰ at 14.5 m, followed by $\delta^{13}C$ values ranging from 1.0 to 1.2‰, and average out at 1.1‰.

The *Nuttallides truempyi* $\delta^{18}O$ values are negative throughout the studied section, showing trends that are similar to those of the $\delta^{13}C$ values. In the lower part of the section (from 1 to 11.5 m), $\delta^{18}O$ values show a decreasing trend towards metre 4, followed by a gradual increase. They range from −1.5‰ to −1.0‰, and average out at −1.2‰. A shift to more negative values is recorded over the interval from 12 to 13.5 m, ranging from −1.4‰ to −1.2‰. The $\delta^{18}O$ record strongly fluctuates over the interval from 14 to 15.25 m in coincidence with the interval R. Only two samples were analysed towards the top of the Caravaca section (from 16 to 18 m), and these show average $\delta^{18}O$ values of −1.1‰.

The benthic species *Nuttallides truempyi* was selected in order to minimise the effect of diagenesis on the stable isotopic composition. Although the apparent correlation between the $\delta^{13}C$ and $\delta^{18}O$ values suggests that *Nuttallides truempyi* may have undergone significant diagenetic overprint, the magnitude of $\delta^{13}C$ values is similar to coeval unaltered pelagic deposits (Zachos et al., 2001) and the $\delta^{13}C$ shift (−0.6‰) is similar to other Paleocene and Eocene hyperthermal events, including the CIE reported across the LDE. These results suggest that $\delta^{13}C$ data from *Nuttallides truempyi* may reflect a primary signal.

3.2. Calcareous nannofossils and biostratigraphy

The calcareous nannofossil content of the Caravaca section was first investigated by Romein (1979), who pointed out the continuous sedimentation of the section, reported a detailed distribution of the calcareous nannofossils and the evolutionary trends of the main genera (in particular of *Fasciculithus*), and recognized the most important zones of the Paleocene. Recent studies on the calcareous nannofossil biostratigraphy across the Danian-Selandian transition include Steurbaut and Sztrákos (2008), Bernaola et al. (2009), Coccioni et al. (2010), Dinarès-Turell et al. (2010), Aubry et al. (2012) and Monechi et al. (2013). Following the standard biostratigraphic zonation of Martini (1971), the studied interval spans the NP4 Zone (Martini, 1971) and Zones NTp6-8 of Varol (1989). In this study, however, we applied the new zonation of Agnini et al. (2014), codified as CNP, integrated with the bio-horizons proposed by Monechi et al. (2013) because it provides a better resolution and easier correlation with other sections.

Preservation of calcareous nannofossils varies from medium to poor, showing traces of dissolution and recrystallisation. Reworked Cretaceous species are present with different abundances throughout the studied interval. The stratigraphic ranges of the most important taxa have been reported in Fig. 2. The biostratigraphic distribution of index species correlates well with other sections in different paleogeographic settings (Sites 1262 and 577A, and Bottaccione, Contessa, Zumaia, Qreiya and Bijala sections; e.g. Monechi et al., 2013). The presence of *Gomphiolithus magnus* and *G. magnicordis* from the lowest part of the studied interval indicate the lower part of Zone CNP5. A succession of several events has been recognized:

- The highest occurrence (Top) of *Gomphiolithus* spp. at metre 6.50–7.
- The lowest occurrence (Base) of *Diantholitha* spp. around metre 10, just one sample below the Base of *Chiasmolithus bidens* group that in agreement with Agnini et al. (2014) can approximate the base of SubZone NTp7b of Varol (1989).
- The lowest occurrences of *Lithoptychius varolii* and L. *chowii* define the First Radiation of *Lithoptychius* (=fasciculiths of Monechi et al., 2013, and references therein) event that occurs at metre 11.50. According to Monechi et al. (2013), this event approximates the onset of the LDE of Bornemann et al. (2009). Immediately above metre 11.50, a sudden and clear negative excursion of $\delta^{13}C$ and $\delta^{18}O$ suggests that this event corresponds to the LDE (=top Chron C27n Event), although our sampling resolution did not allow identification of its a characteristic double peak in carbon isotopes. Furthermore, Arenillas (2012) recorded the first common abundance of the planktic foraminifer *Morozovella* cf. *albeari* at around metre

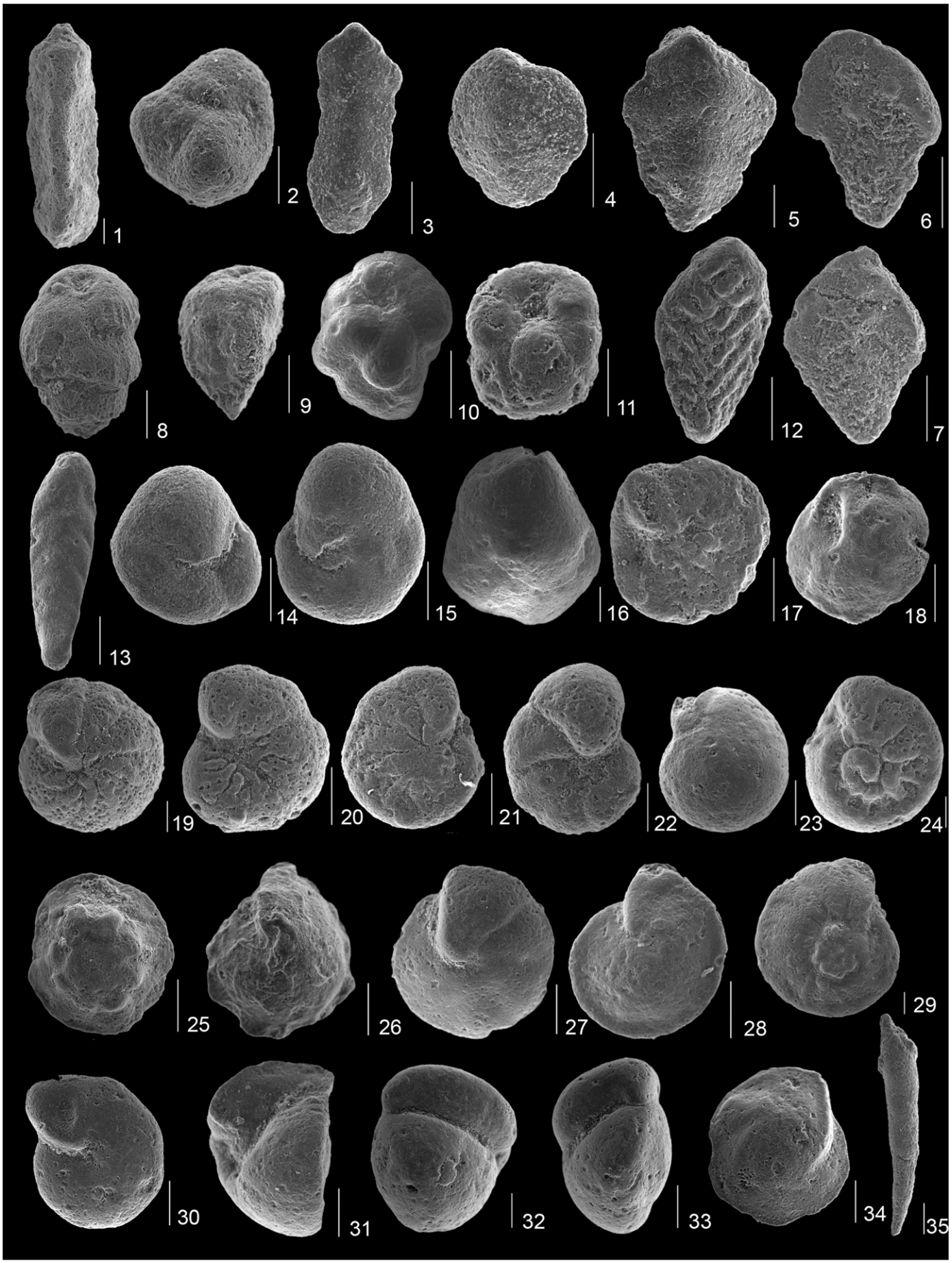
1
2
3
4
5
6
7
8
9
10
11
12
13
14
15
16
17
18
19
20
21
22
23
24
25
26
27
28
29
30
31
32
33
34
35

11.50–12. This is a controversial species that has been commonly included in the taxonomic concept of *Igorina albeari* (Sprong et al., 2009; Arenillas, 2012), but this controversy is outside the scope of this paper. According to Jehle et al. (2015), the first common abundance of this species marks the onset of the LDE, rather than a simple first (rare) common occurrence. Following these authors, one may conclude that planktic foraminifera indicate that the onset of the LDE is located at metre 11.50–12 at Caravaca. This inference is in agreement with our calcareous nannofossil results.

- The lowest common occurrence of *Sphenolithus moriformis* gr. has been identified at metre 16. This event defines the base of CNP7 Zone and can approximate the base of NTp8 Zone. Very rare specimens of *Sphenolithus* have been recorded in two lower samples at metre 12.50 suggesting a lower level for the lowest occurrence of this genus.
- A paracme (absence) of *Lithoptychius* has been recognized across a 2 m-thick interval (from 15.50 to 17.50 m). *Sphenolithus* becomes common across this interval.
- The occurrence of *L. ulii*, *L. janii* and *L. vertebratoides* has been observed at the very top of the section, indicating the recovery of *Lithoptychius* and the beginning of the Second radiation at metre 18.
- *L. billii* has been recorded between metres 20 and 22, and can approximate the Danian/Selandian boundary (Monechi et al., 2013).

An approximately 1-m-thick interval (called "interval R", around metres 14.25–15.25) shows an abrupt and major change in the calcareous nannofossil assemblages. The genera *Braarudosphaera* and *Thoracosphaera*, and Cretaceous specimens increase markedly within this interval, whereas sphenoliths and *Lithoptychius* are absent, and the presence of older and larger forms such as *Gomphiolithus* sp. and *Diantholitha* spp. has been observed. These data suggest that interval R corresponds to a reworked level.

Calcareous nannofossil assemblages show abundant and diversified nannoflora consisting mainly of *Coccolithus pelagicus*, *Prinsius* spp., *Cruciplacolithus tenuis*, *Placozygus sigmoides*, and *Ericsonia subpertusa.* Species of *Braarudosphaera* and *Thoracosphaera* are common in the lower part of the section, while *Toweius pertusus* is sporadically present in the lower part of the section and it occurs from metre 12 upwards. *Ellipsolithus macellus*, the marker species of NP4 Zone, is very rare and it has been observed in very few samples throughout the studied interval.

3.3. Benthic foraminifera

Benthic foraminiferal assemblages from Caravaca are diverse and well preserved. Agglutinated foraminifera are minor components of the assemblages (4–21%; Fig. 2). The high percentages of calcareous taxa indicate deposition well above the carbonate compensation depth. Among calcareous species, *Nuttallides truempyi*, *Bulimina trinitatensis*, *Buliminella beaumonti*, *Cibicidoides hyphalus*, *Stensioeina beccariiformis*, *Oridorsalis umbonatus*, *Anomalinoides ammonoides* and *Coryphostoma midwayensis* are most abundant (Fig. 3). Laevidentalinids, *Lenticulina* spp. and unilocular taxa are also abundant. Other common taxa include *Gyroidinoides* and *Nonion* species. *Spiroplectammina spectabilis* is the most abundant agglutinant species, and it makes up to 8% of the benthic assemblages. *Clavulinoides* and *Marssonella* species are also common among agglutinated taxa. Assemblages are slightly to fairly dominated by infaunal morphogroups (56–76%; Fig. 2), reaching the highest percentages towards the upper part of the section. Taxa with cylindrical-tapered (e.g. buliminids, laevidentalinids), rounded-planispiral (e.g. *Lenticulina* and *Nonion* species), spherical (e.g. *Lagena* species) and tapered-flattened (e.g. *S. spectabilis*) tests dominate among infaunal morphogroups. Among the epifaunal morphogroups, species with planoconvex-trochospiral (e.g. *N. truempyi*, *S. beccariiformis*) and biconvex-trochospiral (e.g. *A. ammonoides*) tests dominate.

The R-mode cluster analysis shows two main clusters (A and B) of benthic foraminifera, and each one is subdivided into two minor assemblages (Figs. 3, 4).

Cluster A (*Gaudryina* spp. – *Anomalinoides* spp.) includes both infaunal and epifaunal taxa, but it is dominated by infaunal species. This cluster is most abundant in the lower half of the section (Fig. 4), and it is divided into subclusters A1 and A2. Subcluster A1 is more abundant in the middle part of the studied section, in the pre-LDE interval. Its abundance drops down to minimum values within the core of the LDE, and shows a positive peak within the upper part of the LDE interval. *Lagena* spp. and *Lenticulina* spp. are the most abundant taxa in this cluster, and *O. umbonatus* and *A. ammonoides* are common. The highest abundance of subcluster A2 is recorded towards the lower part of the section and at the lower part of the LDE interval, and it shows a progressive decrease in relative abundance across de LDE and towards the top of the section, which is only interrupted by an increase across the reworked interval. *N. truempyi* is the most abundant species in A2, and other common species include *B. trinitatensis*, *S. spectabilis* and *C. hyphalus*.

Cluster B (*C.* cf. *pseudoperlucidus-B. beaumonti*) is slightly more abundant in the upper half of the studied section, with abundance peaks being recorded within the LDE interval. Cluster B is divided into subclusters B1 and B2. The first one is most common towards the upper part of the studied section, with marked abundance peaks within the LDE. *Coryphostoma midwayensis*, *S. beccariiformis*, laevidentalinids and polymorphinids are the most abundant taxa in B1. Subcluster B2 is most abundant across the LDE, and it includes the species *Q. allomorphinoides*, *A. aragonensis* and *B. beaumonti*.

The R-mode DCA shows the benthic foraminiferal species mostly concentrated at the centre of the plot (Fig. 5a), but the two main clusters can be easily differentiated. Taxa from cluster B are represented towards the left of the plot, at lower values on axis 1, and species from cluster A show higher values along axis 1. Almost all taxa from the two clusters are located at the same range of values along axis 2, except for *A. aragonensis* from cluster B, which shows higher values along the vertical axis, and *Nuttallinella* spp. from cluster A, placed at the lowest values along this axis.

According to their location in the Q-mode DCA plot (Fig. 5b), the studied samples have been assigned to three main groups: pre-LDE, LDE and reworked intervals. Samples from the pre-LDE interval show higher abundance of species from cluster A, as do samples from the reworked interval. Samples from the LDE interval show strong fluctuations in the abundance of species from subclusters A1, A2 and B1. Species from subcluster B2, which are scarce across the studied section, become more abundant across the LDE interval. Regarding the post-LDE interval, only two samples were analysed (excluding those from the reworked interval): sample 18 m is located at lower values along axis 1 as a result of the high contribution of subcluster B1 to this

Plate 1. Scanning electron micrographs of selected benthic foraminiferal species from Caravaca. All scale bars represent 100 μm. 1 *Clavulinoides trilatera* sample 12.5; 2 *Dorothia crassa*, sample 14; 3 *Spiroplectammina spectabilis*, sample 12; 4 *Spiroplectammina spectabilis*, sample 12; 5 *Spiroplectammina spectabilis*, sample 10.5; 6, *Aragonia aragonensis*, sample 14; 7 *Aragonia aragonensis*, sample 14; 8 *Bulimina trinitatensis*, sample 13; 9 *Bulimina navarroensis*, sample 14; 10 *Buliminella beaumonti*, sample 12.5; 11 *Buliminella grata*, sample 14; 12 *Bolivinoides delicatulus*, sample 13.5; 13 *Coryphostoma midwayensis*, sample 13; 14 *Quadrimorphina allomorphinoides*, sample 12,5; 15, *Quadrimorphina allomorphinoides*, sample 13; 16 *Quadrimorphina allomorphinoides*, sample 1; 17 *Paralabammina hillebrandti*, sample 13; 18 *Paralabammina hillebrandti*, sample 13.5; 19 *Angulogavelinella avnimelechi*, sample 14; 20 *Stensioeina beccariiformis*, sample 14.5; 21, *Cibicidoides howelli*, sample 2; 22 *Cibicidoides hyphalus*, sample 2; 23 *Cibicidoides velascoensis*, sample 13; 24 *Cibicidoides velascoensis*, sample 12.5; 25 *Nuttallides truempyi*, sample 14.5; 26 *Nuttallinella florealis*, sample 10,5; 27 *Oridorsalis umbonatus*, sample 14,5; 28 *Cibicidoides* cf. *pseudoperlucidus*, sample 13.5; 29 *Cibicidoides dayi*, sample 14; 30 *Nonion havanense*, sample 15; 31 *Gyroidinoides girardanus*, sample 14; 32 *Gyroidinoides globosus*, sample 12.5; 33 *Gyroidinoides beisseli*, sample 12.5; 34 *Lenticulina* spp., sample 13; 35 *Laevidentalina* spp., sample 15.

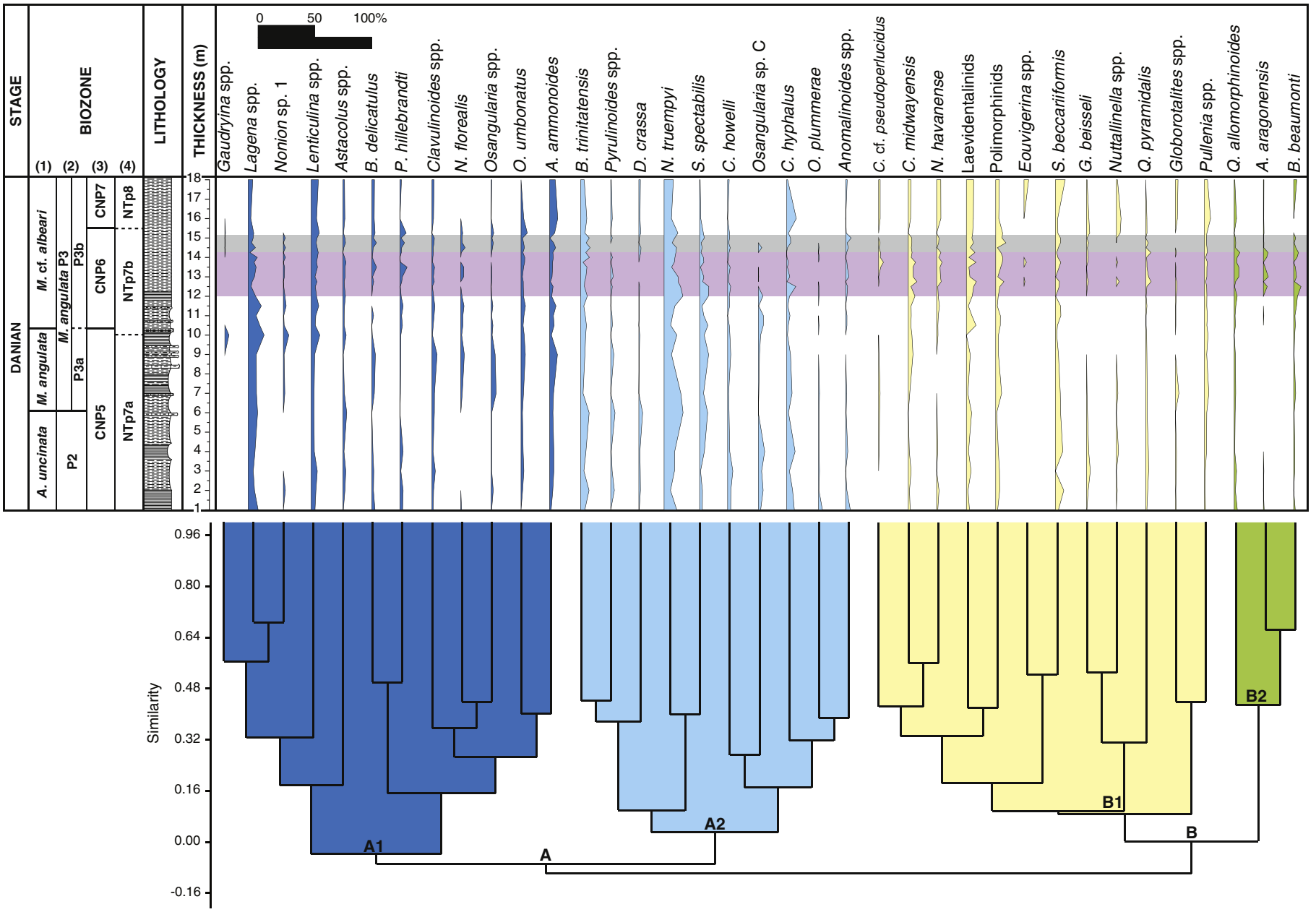

Fig. 3. Cluster analysis plot and relative abundances of selected benthic foraminiferal taxa across the Danian-Selandian transition at Caravaca. Biozones (1) to (4) according to caption for Fig. 2.

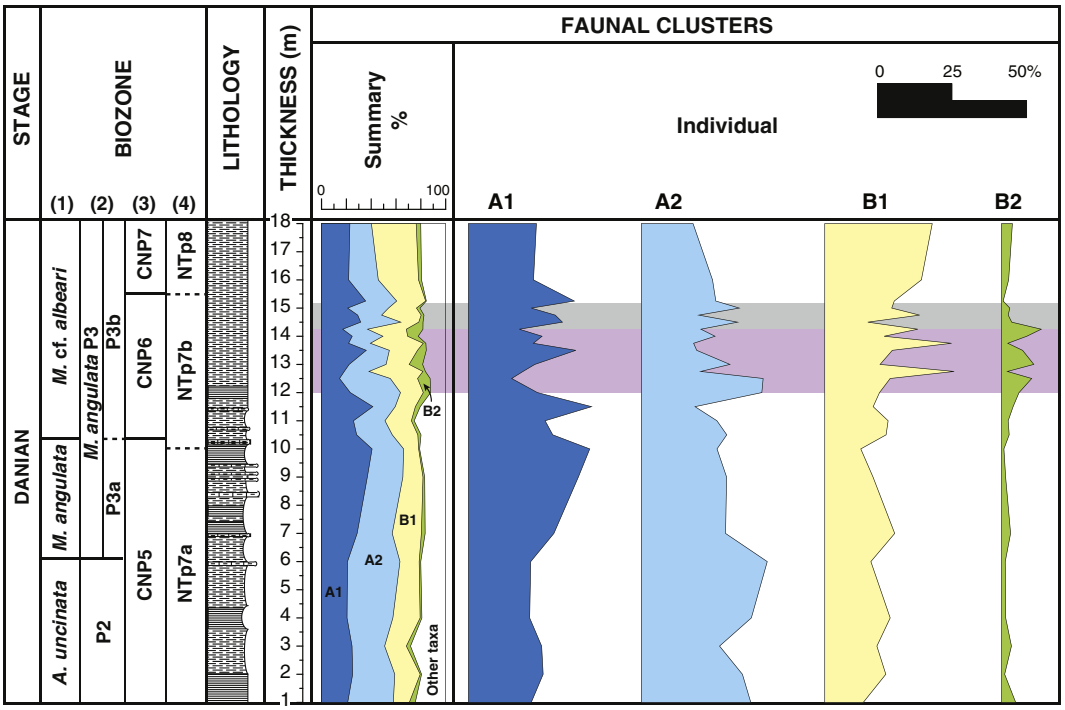

Fig. 4. Relative abundance of benthic foraminiferal clusters across the Danian-Selandian transition at Caravaca. Biozones (1) to (4) according to caption for Fig. 2.

assemblage, and sample 16 m also depicts peaks in abundance of species from subcluster B1.

4. Interpretation and discussion

4.1. Paleobathymetry

Benthic foraminiferal assemblages contain abundant representatives of the bathyal and abyssal Velasco-type fauna (Berggren and Aubert, 1975) namely *Nuttallides truempyi*, *Stensioeina beccariiformis*, *Gyroidinoides globosus*, *Nuttallinella florealis*, *Coryphostoma midwayensis*, *Gaudryina pyramidata*, *Cibicidoides velascoensis*, *Osangularia velascoensis* or *Aragonia velascoensis*, as well as other deep-water species such as *Bulimina trinitatensis*, *Cibicidoides hyphalus*, *Spiroplectammina spectabilis* or *Marssonella oxycona*. The upper depth limit of some of the most abundant species at Caravaca (e.g. *B. trinitatensis*, *N. truempyi*, *S. beccariiformis*, *S. spectabilis*) is located at 500–700 m depth. Shallow-water taxa (e.g. *Oridorsalis plummerae*, *Cibicidoides* cf. *pseudoperlucidus*, *Angulogavelinella avnimelechi*) that are common in sublittoral to upper bathyal depths are also present in Caravaca but they are not common. These data suggest deposition in the middle-lower part of the slope, with no significant changes in paleodepth across the studied section.

4.2. Paleoenvironmental inferences

Benthic foraminiferal assemblages are dominated by infaunal morphogroups throughout the studied section, suggesting mesotrophic to slightly eutrophic conditions at the seafloor (Jorissen et al., 2007) during the late Danian. However, changes in the benthic foraminiferal assemblages and in the isotopic composition of their shells, as well as the calcareous nannofossil turnover, allow us to infer paleoenvironmental changes across the studied interval.

Benthic assemblages from the lower part of the section (biozone CNP5) are mostly dominated by taxa from subcluster A2, such as *N. truempyi* and *S. spectabilis*. Assemblages are relatively stable throughout this interval, but the relative abundance of subcluster A2 increases towards the P2/P3a biozones boundary (samples 6–6.5 m; Fig. 4), coinciding with an increase in the percentage of *N. truempyi* and a decrease in the percentage of *C. hyphalus*. Agglutinated taxa reach their highest abundance within the studied section (20.5%, Fig. 2), and point to slightly carbonate-corrosive bottom waters at the P2/P3a boundary. This hypothesis is supported by a decrease in heterogeneity of the assemblages (Fig. 2), and by the increased abundance of *N. truempyi*, a dissolution-resistant form that thrived during the PETM (Alegret et al., 2009a, 2009b; Giusberti et al., 2009). Increased $CaCO_3$ corrosivity of bottom waters is also consistent with the decreased percentage of some epifaunal taxa such as *C. hyphalus*. Among calcareous nannofossils, the last occurrence of *Gomphiolithus* spp. and a reduction in the hyposaline and opportunistic genus *Braarudosphaera* is recorded in samples 6.5–7 m, which suggests normal salinity conditions and a possible decrease in nutrients (Bartol et al., 2008).

Benthic foraminiferal assemblages undergo significant changes higher up in the section, at the 10 m level, where peaks in abundance of species from subcluster A1 such as unilocular taxa (*Lagena* spp.) and other infaunal taxa (mainly *Lenticulina* spp. and *Nonion* spp.) have been recorded. Increased percentages of infaunal morphogroups in this level may result from an increased nutrient flux to the seafloor (e.g. Jorissen et al., 1995). This interpretation is supported by the decrease in relative abundance of oligotrophic taxa such as *N. truempyi* or *C. hyphalus*. Benthic foraminiferal changes in sample 10 m are coeval with the occurrence of an innovative morphostructure (*Diantholitha)* in the calcareous nannofossil assemblages, which until that time was mainly formed by placoliths. This innovation is difficult to interpret, and it may correspond to a new adaptation to a more efficient biological pump (Fuqua et al., 2008) or to gathering food in a nutrient-poor oceanic water (Aubry et al., 2012). Our data suggests that the first interpretation is more plausible, as a more efficient biological pump would result in an increased nutrient flux to the seafloor, as inferred from benthic foraminifera.

An interval (from ~12 to 14 m) characterised by abundant *Coryphostoma midwayensis* and common *Aragonia aragonensis* and *Quadrimorphina allomorphinoides* has been identified in coincidence with the lowest $\delta^{13}C$ values recorded in the studied section, which mark the LDE. *A. aragonensis* has been speculated to be an opportunistic

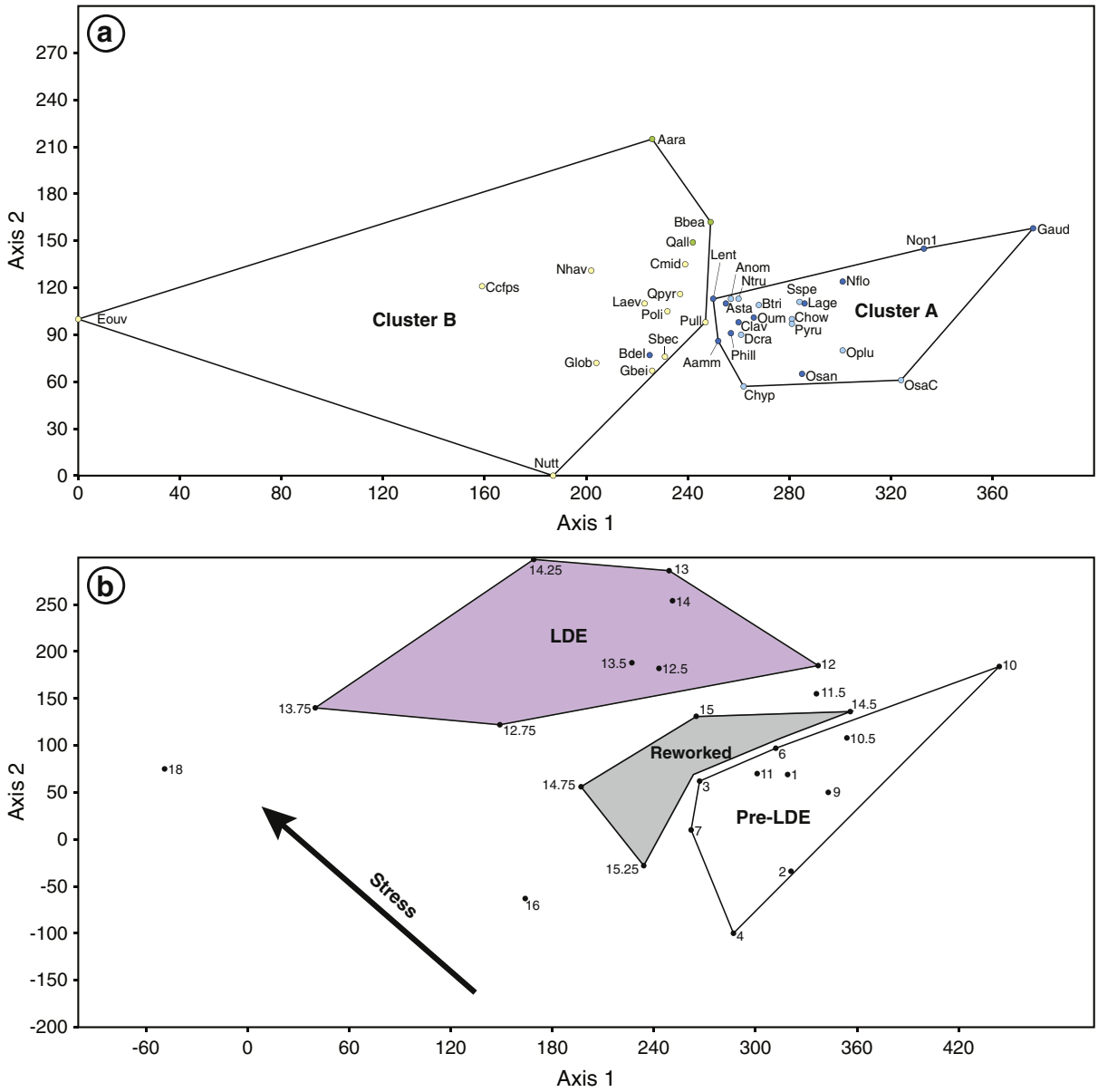

Fig. 5. Detrended Correspondence Analysis results, a) R-mode showing the species distribution, and b) Q-mode showing the location of the studied samples. The arrow indicates the increase in environmental stress based on our interpretation of the data.

species (Steineck and Thomas, 1996) that proliferated in the deep-sea during and after Paleogene warming events (Thomas, 2003; Alegret et al., 2009a; Giusberti et al., 2009; Ortiz et al., 2011; Arreguín-Rodríguez et al., 2016), and is considered as a potential marker of hyperthermal events. Towards the upper part of this interval, assemblages are dominated by infaunal taxa (77% of the assemblages) and contain higher percentages of *Q. allomorphinoides* and buliminids (18% of the assemblages), indicating an increased food flux to the seafloor (Fontanier et al., 2002; Gooday, 2003; Jorissen et al., 2007). Although the total percentage of agglutinated taxa does not increase across the LDE, the increased abundance of calcareous infaunal morphogroups, which calcify in less carbonate-undersaturated pore waters (Foster et al., 2013), and the increased percentages of *N. truempyi*, may point to slightly corrosive bottom waters.

Immediately above the CIE interval that marks the LDE, anomalous values of $\delta^{13}C$ and $\delta^{18}O$ have been recorded (Fig. 2), benthic foraminiferal assemblages fluctuate as seen in the faunal clusters (Fig. 3), *A. aragonensis* becomes very scarce, and assemblages of calcareous nannofossils are more similar to those recorded in the lower part of the studied section. These results suggest that this problematic interval corresponds to a reworked interval, possibly through faulting or a slump. The Q-mode DCA plot clearly places the studied samples in three groups (pre-LDE, LDE and reworked intervals; Fig. 5). The consecutive arrangement of these groups may indicate increased environmental stress, with lowest values during the pre-LDE interval, and maximum values during the LDE interval. The reworked interval is plotted very close to the pre-LDE interval, suggesting a strong similarity between benthic foraminiferal assemblages.

The upper part of the studied section corresponds to the post-LDE interval. The percentage of infaunal morphogroups and buliminids decreases above the reworked interval, subcluster B1 increases, and the oligotrophic taxon *Cibicidoides hyphalus* is slightly more abundant, suggesting a slight decrease in the nutrient flux to the seafloor towards the top of the section. Among calcareous nannofossils, *Prinsius* and *Toweius* are common and *Sphenolithus* shows the common occurrence in sample 16 m, where a paracme of *Lithoptychius* has been observed. In agreement with Monechi et al. (2013), these changes suggest a mesotrophic preference for *Sphenolithus* (Wade and Bown, 2006) and slightly

cooler waters, and point to the recovery of environmental conditions after the LDE.

4.3. The latest Danian event

Previous studies on calcareous plankton from shallower settings in the Southern Tethys (Tunisia and Egypt; Guasti et al., 2006; Sprong et al., 2012, 2013) have documented a change from oligotrophic conditions in the P2/P3a transition to shallower and nutrient-rich environments from the base of Subzone P3b. More eutrophic conditions have also been inferred for the benthic realm. Sprong et al. (2012) documented a rapid relative sea-level rise in the Egyptian sections during the LDE, the magnitude of shallowing and subsequent deepening across the LDE not exceeding 50 m maximum, whereas this interval and the P3a/P3b transition are condensed in the Tunisian sections (Sprong et al., 2013). A sea-level fall was also identified across the LDE by Steurbaut and Sztrákos (2008), who examined sections from the southern Tethys up to the North Sea Basin. Our results support an increase in the food supply towards the base of Subzone P3b, and a further increase towards the top of the CIE that marks the LDE, but no changes in paleodepth have been inferred at Caravaca. We cannot exclude, however, minor sea-level changes which might not be detectable through the vertical depth-distribution of benthic foraminifera in such a deep (middle-lower bathyal) environment. The planktic turnover shares similarities between the Southern Tethyan sections and Caravaca, such as the radiation of *Lithoptychius* among calcareous nannofossils, and the substitution of the planktic foraminiferal genus *Praemurica* by *Morozovella* (reported from the Caravaca section by Arenillas and Molina, 1997 and Arenillas, 2012). The replacement of *Praemurica* by *Morozovella* was also documented from the Southern Tethys (Tunisia) by Guasti et al. (2006) and from Pacific ODP Site 1210 by Jehle et al. (2015).

In addition, changes in benthic foraminiferal assemblages across the LDE at Caravaca share some characteristics with other hyperthermal events (e.g., PETM, ETM2, H2, ETM3), such as the negative shift in the carbon isotopic signal in their calcareous tests, the common occurrence of *A. aragonensis*, or the increased abundance of buliminids towards the upper part of this event, which may indicate unfavourable conditions, fluctuations in food supply to the seafloor, or increased $CaCO_3$ corrosivity of bottom waters (e.g. Thomas, 2007; Alegret et al., 2009a, 2009b; Arreguín-Rodríguez et al., 2016; Arreguín-Rodríguez and Alegret, 2016).

Benthic foraminiferal changes did not start in coincidence with the onset of the CIE that marks the LDE at Caravaca, but more gradually below this onset, as observed in the gradual increase in % buliminids and other calcareous infaunal taxa (Figs. 2, 3), or the decrease in heterogeneity of the assemblages (Fig. 2). These results point to an early onset of the biotic and paleoenvironmental perturbations, which started before the onset of the LDE, in agreement with Jehle et al. (2015).

5. Conclusions

Micropaleontological and geochemical studies of upper Danian sediments from the bathyal Caravaca section (Spain) allowed us to identify calcareous nannofossil biozones and to evaluate the paleoenvironmental turnover in the western Tethyan realm. The Latest Danian Event (LDE) at Caravaca has been identified within calcareous nannofossil and planktic foraminiferal Subzones NTp7b and P3b, respectively, in coincidence with a negative shift in benthic foraminiferal $\delta^{13}C$ values and significant changes in planktic assemblages. The First Radiation of *Lithoptychius* (= fasciculiths) approximates the onset of the LDE.

Changes in benthic foraminiferal assemblages did not start sharply at the onset of the carbon isotope excursion that marks the LDE, but gradually below this interval. The occurrence of innovative morphostructures (*Diantholitha*) in the calcareous nannofossil assemblages, increased percentages of benthic infaunal morphogroups and a decrease in the abundance of benthic oligotrophic species, indicate a more efficient biological pump during the LDE. In addition, the increased abundance of benthic taxa that are resistant to dissolution suggests slightly more corrosive bottom waters during this event. The composition of the benthic assemblages across this event has similarities with the assemblages across other Paleocene and Eocene hyperthermal events.

Acknowledgements

The authors acknowledge funding from projects CGL2014-58794-P (Spanish Ministry of Economy and Competitiveness and FEDER funds), Consolidated Group E05 (Government of Aragon/European Social Fund), and MIUR-PRIN grant 2010X3PP8J_005. G.J.A.R. thanks the Consejo Nacional de Ciencia y Tecnología (Conacyt, México) for her predoctoral fellowship.

References

Agnini, C., Fornaciari, E., Raffi, I., Catanzariti, R., Pälike, H., Backman, J., Rio, D., 2014. Biozonation and biochronology of Paleogene calcareous nannofossils from low and middle latitudes. Newsl. Stratigr. 47 (2), 131–181.

Alegret, L., Ortiz, S., 2010. El corte de Zumaya (España): registro de los foraminíferos bentónicos del Paleógeno inferior. Revista Mexicana de Ciencias Geológicas 27, 477–489.

Alegret, L., Ortiz, S., 2013. Uppermost cretaceous to lowermost Eocene benthic foraminifera of the Dababiya Corehole, upper Nile Valley, Egypt. Stratigraphy 9 (3–4), 267–277.

Alegret, L., Thomas, E., 2001. Upper cretaceous and lower Paleogene benthic foraminifera from northeastern Mexico. Micropaleontology 47 (4), 269–316.

Alegret, L., Ortiz, S., Orue-Etxebarria, X., Bernaola, G., Baceta, J.I., Monechi, S., Apellaniz, E., Pujalte, V., 2009a. The Paleocene–Eocene Thermal Maximum: New Data from the Microfossil Turnover at Zumaia Section: Palaios. Vol. 24 pp. 318–328.

Alegret, L., Ortiz, S., Molina, E., 2009b. Extinction and recovery of benthic foraminifera across the Paleocene-Eocene thermal maximum at the Alamedilla section (southern Spain). Palaeogeogr. Palaeoclimatol. Palaeoecol. 279, 186–200.

Alegret, L., Ortiz, S., Arenillas, I., Molina, E., 2010. What happens when the ocean is overheated? The foraminiferal response across the Paleocene-Eocene thermal maximum at the Alamedilla section (Spain). Geol. Soc. Am. Bull. 122, 1616–1624.

Arenillas, I., 2012. Patterns of spatio-temporal distribution as criteria for the separation of planktic foraminiferal species across the Danian-Selandian transition in Spain. Acta Palaeontol. Pol. 57 (2), 401–422.

Arenillas, I., Molina, E., 1997. Análisis cuantitativo de los foraminíferos planctónicos del Paleoceno de Caravaca (Cordillera Bética): bioestratigrafía y evolución de las asociaciones. Revista Española de Paleontología 12 (2), 207–232.

Arreguín-Rodríguez, G.J., Alegret, L., 2016. Deep-sea benthic foraminiferal turnover across early Eocene hyperthermal events at Northeast Atlantic DSDP site 550. Palaeogeogr. Palaeoclimatol. Palaeoecol. 451, 62–72.

Arreguín-Rodríguez, G.J., Alegret, L., Thomas, E., 2016. Late Paleocene – middle Eocene benthic life on a Pacific seamount (Allison Guyot, ODP site 865): greenhouse climate and superimposed hyperthermal events. Paleoceanography http://dx.doi.org/10.1002/2015PA002837.

Aubry, M.P., Rodriguez, O., Bord, D., Godfrey, L., Schmitz, B., Knox, R.W.O.'.B., 2012. The first radiation of the fasciculiths: morphologic adaptations of the coccolithophores to oligotrophy. Austrian Journal of Earth Sciences 105 (1), 29–38.

Bartol, M., Pavšič, J., Dobnikar, M., Bernasconi, S.M., 2008. Unusual *Braarudosphaera bigelowii* and *Micrantholithus vesper* enrichment in the early Miocene sediments from the Slovenian corridor, a seaway linking the central Paratethys and the Mediterranean. Palaeogeogr. Palaeoclimatol. Palaeoecol. 267, 77–88.

Berggren, W.A., Aubert, J., 1975. Paleocene benthonic foraminiferal biostratigraphy, paleobiogeography and paleoecology of Atlantic–Tethyan regions: midway-type fauna. Palaeogeogr. Palaeoclimatol. Palaeoecol. 18, 73–192.

Berggren, W.A., Pearson, P.N., 2005. A revised tropical to subtropical Paleogene planktonic foraminiferal zonation. J. Foraminifer. Res. 35, 279–298.

Bernaola, G., Baceta, J.I., Orue-Etxebarria, X., Alegret, L., Martin, M., Arostegui, J., Dinarès, J., 2007. Evidence of an abrupt environmental disruption during the mid Paleocene biotic event (Zumaia section, W Pyrenees). Geol. Soc. Am. Bull. 119 (7), 785–795.

Bernaola, G., Martin-Rubio, M., Baceta, J.I., 2009. New high resolution calcareous nannofossil analysis across the D/S transition at the Zumaia section: comparison with south Tethys and Danish sections. Geol. Acta 7 (1–2), 79–92.

Bornemann, A., Schulte, P., Sprong, J., Steurbaut, E., Youssef, M., Speijer, R.P., 2009. Latest Danian carbon isotope anomaly and associated environmental change in the southern Tethys (Nile basin, Egypt). J. Geol. Soc. 166, 1135–1142.

Bowen, G.J., Maibauer, B.J., Kraus, M.J., Röhl, U., Westerhold, T., Steimke, A., Gingerich, P.D., Wing, S.L., Clyde, W.C., 2014. Two massive, rapid releases of carbon during the onset of the Palaeocene–Eocene thermal maximum. Nat. Geosci. 8, 44–47.

Coccioni, R., Frontalini, F., Bancalà, G., Fornaciari, E., Jovane, L., Sprovieri, M., 2010. The Dan-C2 hyperthermal event at Gubbio (Italy): global implications, environmental effects, and cause(s). Earth Planet. Sci. Lett. 297, 298–305.

Corliss, B.H., Chen, C., 1988. Morphotype patterns of Norwegian Sea deep-sea benthic foraminifera and ecological implications. Geology 16, 716–719.

DeConto, R.M., Galeotti, S., Pagani, M., Tracy, D., Schaefer, K., Zhang, T., Pollard, D., Beerling, D.J., 2012. Past extreme warming events linked to massive carbon re-lease from thawing permafrost. Nature 484, 87–92.

Dickens, G.R., O'Neil, J.R., Rea, D.K., Owen, R.M., 1995. Dissociation of oceanic methane hydrate as a cause of the carbon isotope excursion at the end of the Paleocene. Paleoceanography 10, 965–971.

Dinarès-Turell, J., Stoykova, K., Baceta, J.I., Ivanov, M., Pujalte, V., 2010. High-resolution intra and interbasinal correlation of the Danian–Selandian transition (early Paleocene): the Bjala section (Bulgaria) and the Selandian GSSP at Zumaia (Spain). Palaeogeogr. Palaeoclimatol. Palaeoecol. 297 (2), 511–533.

Dinarès-Turell, J., Pujalte, V., Stoykova, K., Baceta, J.I., Ivanov, M., 2012. The Palaeocene "top chron C27n" transient greenhouse episode: evidence from marine pelagic Atlantic and peri-Tethyan sections. Terra Nova 24, 477–486.

Dinarès-Turell, J., Westerhold, T., Pujalte, V., Röhl, U., Kroon, D., 2014. Astronomical calibration of the Danian stage (early Paleocene) revisited: settling chronologies of sedimentary records across the Atlantic and Pacific oceans. Earth Planet. Sci. Lett. 405, 119–131. http://dx.doi.org/10.1016/j.epsl.2014.08.027.

Dunkley-Jones, T., Lunt, D.J., Schmidt, D.N., Ridgwell, A., Sluijs, A., Valdes, P.J., Maslin, M., 2013. Climate model and proxy data constraints on ocean warming across the Paleocene–Eocene thermal maximum. Earth Sci. Rev. 125, 123–145.

Fontanier, C., Jorissen, F.J., Licari, L., Alexandre, A., Anschutz, P., Carbonel, P., 2002. Live benthic foraminiferal faunas from the Bay of Biscay: faunal density, composition and microhabitats. Deep-Sea Research I 49, 751–785.

Foster, L.C., Schmidt, D.N., Thomas, E., Arndt, S., Ridgwell, A., 2013. Surviving rapid climate change in the deep sea during the Paleogene hyperthermals. PNAS 110 (23), 9273–9276.

Fuqua, L.M., Bralower, T.J., Arthur, M.A., Patzkowsky, M.E., 2008. Evolution of calcareous nannoplankton and the recovery of marine food webs after the cretaceous- Paleocene mass extinction. Palaios 23, 185–194.

Giusberti, L., Coccioni, R., Sprovieri, M., Tateo, F., 2009. Perturbation at the sea floor during the Paleocene–Eocene thermal maximum: evidence from benthic foraminifera at Contessa road, Italy. Mar. Micropaleontol. 70, 102–119.

Gooday, A.J., 2003. Benthic foraminifera (Protista) as tools in deep-water paleoceanography: environmental influences on faunal characteristics. Adv. Mar. Biol. 46, 1–90.

Guasti, E., Kouwenhoven, T.J., Brinkhuis, H., Speijer, R.P., 2005. Paleocene Sea-level and productivity changes at the southern Tethyan margin (el kef, Tunisia). Mar. Micropaleontol. 55, 1–17.

Guasti, E., Speijer, R.P., Brinkhuis, H., Smit, J., Steurbaut, E., 2006. Paleoenvironmental change at the Danian–Selandian transition in Tunisia: planktic foraminifera and organic-walled dinoflagellate cysts records. Mar. Micropaleontol. 59, 210–229.

Hammer, Ø., Harper, D.A.T., Ryan, P.D., 2001. PAST: paleontological statistics software package for education and data analysis. Palaeontol. Electron. 4 (1), 1–9.

Higgins, J.A., Schrag, D.P., 2006. Beyond methane: towards a theory for the Paleocene–Eocene thermal maximum. Earth Planet. Sci. Lett. 245, 523–537.

Jehle, S., Bornemann, A., Deprez, A., Speijer, R.P., 2015. The impact of the latest Danian event on planktic foraminiferal faunas at ODP site 1210 (Shatsky rise, Pacific Ocean). PLoS One 10 (11), e0141644. http://dx.doi.org/10.1371/journal.pone.0141644.

Jorissen, F.J., De Stigter, H.C., Widmark, J.G.V., 1995. A Conceptual Model Explaining Benthic Foraminifera Microhabitats. In: Langer, M.R. (Ed.), FORAMS 1994. Marine Micropaleontology Vol. 26, pp. 3–15.

Jorissen, F.J., Fontanier, C., Thomas, E., 2007. Paleoceanographical Proxies Based on Deep-Sea Benthic Foraminiferal Assemblages Characteristics. In: Hillaire-Marcel, C., Vernal, A. (Eds.), Proxies in Late Cenozoic Paleoceanography: Part 2: Biological Tracers and Biomarkers. Elsevier, Amsterdam, pp. 263–326.

Kurtz, A., Kump, L.R., Arthur, M.A., Zachos, J.C., Paytan, A., 2003. Early Cenozoic de-coupling of the global carbon and Sulphur cycles. Paleoceanography 18, 1090. http://dx.doi.org/10.1029/2003PA000908.

Lauretano, V., Littler, K., Polling, M., Zachos, J.C., Lourens, L.J., 2015. Frequency, magnitude and character of hyperthermia; events at the onset of the early Eocene climatic optimum. Clim. Past Discuss. 11, 1795–1820.

Littler, K., Röhl, U., Westerhold, T., Zachos, J.C., 2014. A high-resolution benthic stable-isotope record for the South Atlantic: implications for orbital-scale changes in late Paleocene-early Eocene climate and carbon cycling. Earth Planet. Sci. Lett. 401, 18–30.

Loeblich, A.R.J., Tappan, H., 1987. Foraminifera Genera and their Classification. Van Nostrand Reinhold Company Inc., New York.

Lourens, L.J., Sluijs, A., Kroon, D., Zachos, J.C., Thomas, E., Röhl, U., Bowles, J., Raffi, I., 2005. Astronomical pacing of late Palaeocene to early Eocene global warming events. Nature 435, 1083–1087.

Martini, E., 1971. Standard Tertiary and Quaternary Calcareous Nannoplankton Zonation. Proceedings II Planktonic Conference, Roma, Italy, pp. 739–785.

McCarren, H., Thomas, E., Hasegawa, T., Röhl, U., Zachos, J.C., 2008. Depth dependency of the Paleocene–Eocene carbon isotope excursion: paired benthic and terrestrial biomarker records (ocean drilling program leg 208, Walvis ridge). Geochem. Geophys. Geosyst. 9, Q10008. http://dx.doi.org/10.1029/2008GC002116.

Molina, E., 1994. Paleocene sections in Spain: chronostratigraphical problems and possibilities. GFF 116 (1), 58–60.

Monechi, S., Reale, V., Bernaola, G., Balestra, B., 2012. Taxonomic review of early Paleocene fasciculiths. Micropaleontology 58 (4), 351–356.

Monechi, S., Reale, V., Bernaola, G., Balestra, B., 2013. The Danian/Selandian boundary at site 1262 (South Atlantic) and in the Tethyan region: Biomagnetostratigraphy, evolutionary trends in fasciculiths and environmental effects of the latest Danian event. Mar. Micropaleontol. 98, 28–40.

Nicolo, M.J., Dickens, G.R., Hollis, C.J., Zachos, J.C., 2007. Multiple early Eocene hyperthermals: their sedimentary expression on the New Zealand continental margin and in the deep sea. Geology 35, 699–702.

Nisbet, E.G., Jones, S.M., Maclennan, J., Eagles, G., Moed, J., Warwick, N., Bekki, S., Braesicke, P., Pyle, J.A., Fowler, C.M.R., 2009. Kick-starting ancient global warming. Nat. Geosci. 2, 156–159.

Ortiz, S., Alegret, L., Arenillas, I., Molina, E., 2008. Análisis de las asociaciones de foraminíferos del tránsito Daniense-Selandiense en Caravaca (Murcia). Geotimes 10, 1479–1482.

Ortiz, S., Alegret, L., Payros, A., Orue-Etxebarria, X., Apellaniz, E., Molina, E., 2011. Distribution patterns of benthic foraminifera across the Ypresian-Lutetian Gorrondatxe section, northern Spain: response to sedimentary disturbance. Mar. Micropaleontol. 78, 1–13.

Perch-Nielsen, K., Saunders, J.B., 1985. Cenozoic calcareous nannofossils. In: Bolli, H.M., Perch-Nielsen, K. (Eds.), Plankton Stratigraphy Vol. 11. Cambridge Earth Science Series, Cambridge, pp. 427–554.

Petrizzo, M.R., 2005. An early late Paleocene event on Shatsky rise, Northwest Pacific Ocean (ODP leg 198): evidence from planktonic foraminiferal assemblages. Proc. ODP Sci. Results 198, 1–29.

Quillévéré, F., Norris, R.D., 2003. In: Wing, S.L., Gingerich, P.D., Schmitz, B., Thomas, E. (Eds.), Ecological Development of Acarininids (Planktonic Foraminifera) and Hydrographic Evolution of Paleocene Surface Waters. Geological Society of America Special Paper 369, Boulder, CO, pp. 223–238.

Quillévéré, F., Norris, R.D., Kroon, D., Wilson, P.A., 2008. Transient Ocean warming and shifts in carbon reservoirs during the early Danian. Earth Planet. Sci. Lett. 265, 600–615. http://dx.doi.org/10.1016/j.epsl2007.10.040.

Röhl, U., Bralower, T.J., Norris, G., Wefer, G., 2000. A new chronology for the late Paleocene thermal maximum and its environmental implications. Geology 28, 927–930.

Romein, A.J.T., 1979. Lineages in Early Paleogene Calcareous Nannoplankton. Utrecht Micropalaeontological Bulletin 22, Utrecht 230 p.

Schmitz, B., Molina, E., von Salis, K., 1998. The Zumaya section in Spain: a possible global stratotype section for the Selandian and Thanetian stages. Newsl. Stratigr. 36 (1), 35–42.

Schmitz, B., Pujalte, V., Molina, E., Monechi, S., Orue-Etxebarria, X., Alegret, L., Apellaniz, E., Arenillas, I., Aubry, M.P., Baceta, J.I., Berggren, W., Bernaola, G., Caballero, F., Clemmensen, A., Dinarès-Turell, J., Dupuis, C., Heilmann-Clausen, C., Hilario, A., Knox, R., Martín-Rubio, M., Ortiz, S., Payros, A., Petrizzo, M.R., von Salis, K., Speijer, R., Sprong, R., Steurbaut, E., Thomsen, E., 2011. The global boundary stratotype sections and points for the bases of the Selandian (middle Paleocene) and Thanetian (upper Paleocene) stages at Zumaia, Spain. Episodes 34 (4), 220–243.

Speijer, R., 2003. Danian–Selandian Sea-Level Change and Biotic Excursion on the Southern Tethyan Margin. In: Wing, S.L., Gingerich, P.D., Schmitz, B., Thomas, E. (Eds.), Causes and Consequences of Globally Warm Climates in the Early Paleogene. Geological Society of America Special Paper 369, Boulder, CO, pp. 275–290.

Speijer, R.P., Schmitz, B., 1998. A benthic foraminiferal record of Paleocene Sea level and trophic/redox conditions at Gebel Aweina, Egypt. Palaeogeogr. Palaeoclimatol. Palaeoecol. 137, 79–101.

Sprong, J., Speijer, R.P., Steurbaut, E., 2009. Biostratigraphy of the Danian/Selandian transition in the southern Tethys. Special reference to the lowest occurrence of planktic foraminifera *Igorina albeari*. Geol. Acta 7 (1–2), 63–77.

Sprong, J., Kouwenhoven, T.J., Bornemann, A., Schulte, P., Steurbaut, E., Youssef, M., Speijer, R.P., 2012. Characterization of the latest Danian event by means of benthic foraminiferal assemblages along a depth transect at the southern Tethyan margin (Nile Basin, Egypt). Mar. Micropaleontol. 86–87, 15–31.

Sprong, J., Kouwenhoven, T.J., Bornemann, A., Dupuis, C., Speijer, R.P., Stassen, P., Steurbaut, E., 2013. In search of the latest Danian event in a paleobathymetric transect off Kasserine Island, north-Central Tunisia. Palaeogeogr. Palaeoclimatol. Palaeoecol. 379–380, 1–16.

Stap, L., Lourens, L.J., Thomas, E., Sluijs, A., Bohaty, S., Zachos, J.C., 2010. High-resolution deep-sea carbon and oxygen isotope records of Eocene thermal maximum 2 and H2. Geology 38, 607–610.

Steineck, P.L., Thomas, E., 1996. The latest Paleocene crisis in the deep sea: Ostracode succession at Maud rise, Southern Ocean. Geology 24, 583–586.

Steurbaut, E., Sztrákos, K., 2008. Danian/Selandian boundary criteria and North Sea basin-Tethys correlations based on calcareous nannofossil and foraminiferal trends in SW France. Mar. Micropaleontol. 67, 1–29.

Svensen, H., Planke, S., Malthe-Sorenssen, A., Jamtveit, B., Myklebust, R., Eidem, T.R., Rey, S.S., 2004. Release of methane from a volcanic basin as a mechanism for initial Eocene global warming. Nature 429, 524–527.

Thomas, E., 2003. Extinction and Food at the Seafloor: A High-Resolution Benthic Foraminiferal Record across the Initial Eocene Thermal Maximum, Southern Ocean Site 690. In: Wing, S.L., Gingerich, P.D., Schmitz, B., Thomas, E. (Eds.), Causes and Consequences of Globally Warm Climates in the Early Paleogene. Geological Society of America Special Paper 369, Boulder, CO, pp. 319–332.

Thomas, E., 2007. Cenozoic Mass Extinctions in the Deep Sea: What Disturbs the Largest Habitat on Earth? In: Monechi, S., Coccioni, R., Rampino, M. (Eds.), Large Ecosystem Perturbations: Causes and Consequences. Geological Society of America Special Paper 424, Boulder, CO, pp. 1–24

Thomas, E., Zachos, J.C., 2000. Was the late Paleocene thermal maximum a unique event? GFF 122, 169–170.

Tjalsma, R.C., Lohmann, G.P., 1983. Paleocene-Eocene bathyal and abyssal benthic foraminifera from the Atlantic Ocean. 4. Micropaleontology Special Publication, pp. 1–89.

Van Morkhoven, F.P.C.M., Berggren, W.A., Edwards, A.S., 1986. Cenozoic Cosmopolitan Deep-Water Benthic Foraminifera. Bulletin des Centres de Recherche Exploration-Production Elf-Aquitaine Memoir 11, Pau, France, pp. 1–421.

Varol, O., 1989. Palaeocene calcareous nannofossil biostratigraphy. In: Crux, J.A., Van Heck, S.E. (Eds.), Nannofossils and their Applications. British Micropaleontological Society Serires Vol. 12, pp. 267–310.

Vera, J.A., 1983. La Cordillera Bética. Las Zonas Externas de las Cordilleras Béticas. Vol. 2. Libro Jubilar J.M. Ríos, Instituto Geológico y Minero Español, Geología de España, pp. 218–251.

Wade, B.S., Bown, P.R., 2006. Calcareous nannofossils in extreme environments: the Messinian salinity crisis, Polemi Basin, Cyprus. Palaeogeogr. Palaeoclimatol. Palaeoecol. 233, 271–286.

Westerhold, T., Roehl, U., Raffi, I., Forniaciari, E., Monechi, S., Reale, V., Bowles, J., Evans, H.F., 2008. Astronomical calibration of the Paleocene time. Palaeogeogr. Palaeoclimatol. Palaeoecol. 257, 377–403.

Westerhold, T., Röhl, U., Donner, B., McCarren, H.K., Zachos, J.C., 2011. A complete high-resolution Paleocene benthic stable isotope record for the Central Pacific (ODP site 1209). Paleoceanography 26, PA2216. http://dx.doi.org/10.1029/2010PA002092.

Zachos, J.C., Pagani, M., Sloan, L.C., Thomas, E., Billups, K., 2001. Trends, rhythms, and aberrations in global climate 65 Ma to present. Science 292, 686–693.

Zachos, J.C., Schouten, S., Bohaty, S.M., Quattlebaum, T., Sluijs, A., Brinkhuis, H., Gibbs, S.J., Bralower, T.J., 2006. Extreme warming of the mid-latitude coastal ocean during the Paleocene–Eocene thermal maximum: inferences from TEX86 and isotope data. Geology 34, 737–740.